

Interpretable Semiotics Networks Representing Awareness

David Kupeev^{*1} and Eyal Nitcany²

¹Independent Researcher, Israel: kupeev@gmail.com

²Independent Researcher, Israel: eyalni@gmail.com

Abstract

Humans perceive objects daily and communicate their perceptions using various channels. Here, we describe a computational model that track and simulate objects' perception, and their representations as they pass in communication.

We describe two key components of our internal representation ('observed' and 'seen') and relate them to familiar computer vision terms (encoding and decoding). These elements joined together to form semiotic networks, which simulate awareness in object perception and human communication.

Nowadays, most neural networks are uninterpretable. On the other hand, our model is free from this disadvantages. We performed several experiments and demonstrated the visibility of our model.

We describe how our network may be used as preprocessing unit to any classification network. In our experiments the compound network overperforms in average the classification network at datasets with small training data.

Future work would leverage our model to gain better understanding of human communications and personal representations.

Keywords: network awareness, network interpretability, semiotics, dialog, perceptual classifier, limited training data

Contents

1 Introduction

3

^{*}Corresponding Author

2	Related Work	5
3	Modeling Person-Person and Person-Object Communication using Semiotic Networks	7
4	Implementation of Semiotics Networks Using Convolutional Autoencoder	9
4.1	Perception of an object by one person: attractors	10
4.2	Perception of an object by two persons: bipartite orbits	11
4.2.1	Bipartite orbits of the first type	12
4.2.2	Bipartite orbits of the second type	17
5	Attractors-based classifier	20
5.1	Vanilla classifier	20
5.2	Stochastic classifier	23
6	Semiotics Interpretation of the model	26
6.1	Perception of a visual object by a person	27
6.2	Person to person communication	29
7	Experimental Results	32
7.1	Implementation of Algorithm 1 for person-to-person communication	32
7.1.1	Attractors	32
7.1.2	Bipartite Orbits	33
7.2	Classifiers	33
8	Discussion and Further Work	40
A	Definition of the sequence U of the images transmuted between the persons in person-to-person CONN implemented using encoder/decoder operations	48
B	Partitioning a subsequence of U	49
C	Proof of Statement 4.3	49
D	Derivation of Eq. 29 from analysis of the meanings a statement.	50
E	Proof of Statement 4.6 (See page 18.)	50

F	Resilience to adversarial attacks of vanilla CONN classifier	52
----------	---	-----------

G	Details of Training Overparameterized Autoencoders at Restricted RMNIST Datasets	53
----------	---	-----------

1 Introduction

Perception of objects by persons can be thought of as an internal representation of the outer world, which can be communicated via various modalities (e.g., text, sound, vision, etc.). Furthermore, the same object can be described in different channels. For example, an image of a dog, or barking sound would set us to believe that a dog is around.

Perception had a few properties, which are in general agnostic to the modality of the perceived input channel. First, perception is mostly subjective. This means that a specific object that is perceived in on manner, may be perceived differently by another person. In other words, two persons may have different internal representation of the same object. For example, two persons that see a dog might think that this is a nice dog (the first person) or a frighten dog (the second). Although, they both 'observe' the same object (dog), they attend to different properties and thus may 'see' other aspects of it. These 'observe' and 'seen' representations are the building block in our model and are used to mimic human perception. They enable one to observe an object and transform ('see') it. Furthermore, this process can be identified also when only a single person is involved. We call it an 'internal cycle', and it occurs during the process of perception of an object. During this process, an object is being perceived (observed), projected onto the 'internal space' ('seen') and then this representation is being used as an observed input to generate another internal representation in a cycle, till a termination of the perception act. It all happens internally and thus can reflect changes that are seen from the outside with regards to the internal representation of an object perceived by a person.

We note that similar process occurs for different modalities such as text, sound, visual (image), etc. and when various modalities are combined. For example, when sound and image are involved together to generate a perception. This may occur for example, when a person hears barks and then after a while sees a dog and conclude that this dog was barking.

Note that the internal personal representation is not revealed. Yet, another abstract level is used and serve as a common basis for communication between persons/systems.

People are very good in object perception under various conditions. For example, you can probably identify your car under different light conditions, and some would be able to recognize their car just by hearing its “unique” soundings. Computer vision algorithms that are specialize in classification would like to possess such a property and indeed many neural networks are trained with various inputs and are agnostic to many differences such as light, rotation, etc.

The mathematical model of human communication presented in this article was developed to represent the existance of the objects seen by a person, as well as the existence of objects the person is aware of them as the seen. Further the mathematical relations have been obtained describing other semiotic phenomena of human-object and human-human communication (Sec. 6). It worth to note that initially, these new aspects were not the focus of our attention. The ability to describe supplementary semiotic phenomena testifies to effectiveness of the model.

The contributions of this paper are as follows:

- Up to our understanding our research is the first attempt to model image visual perception jointly with the the derived inter-person communication [35].
- We model human perception using a sequence of 'observed' and 'seen' personalized images. This provide actual interpretability of the states of the modeling network.
- Through the paper we consider communication either between person or internally 'in the person'. However, 'person' should be interpreted in general sense, meaning to be any sort of system including computer system. On the same note, the processes described in this paper support both internal and external communication through a unified equation. The details for implementing in different systems (e.g. internal representation of object in a person, or communication between two persons) can differ.
- We model the 'observed to seen' operation as composition of encoder and decoder operations of convolution autoencoders. This allows to represent an act of he object perception as a sequence of iterations converging to attractor [28].
- Our model describes several semiotics phenomena of person-object and person to person communication.

- Up to our understanding we introduce the notion of bipartite orbits in dynamics systems.
- We develop an attractor based stochastic classifier for classical computer vision classification tasks. The classifier is interpretable and shows promising performance compared to standard methods, when dealing with limited training datasets.

2 Related Work

Surprisingly, there is limited research available on simulating person-to-person communication. Osgood-Schramm [15] introduces a cyclic model of communication between humans. In their encoder-decoder fashion model, the encoder outputs serve as the transmitted images. In contrast, our model takes a different approach by utilizing encoder outputs as an internal representation of an individual’s input perception.

A few years ago, Google introduced the DeepDream network [23], which bears some resemblance to our work in terms of the concept of observed and seen images and the cycle between them. In their work, the images representing what a person sees in the input image are treated as input to the network. In our work, on the other hand, we simulate the seen images as the network’s output. This fundamental difference accounts for the fact that while delving deep into DeepDream often produces unrealistic ‘dream’ images, our approach tends to generate more realistic ‘normal’ images. Additionally, DeepDream can be viewed as representing one person within our context, where its observe-seen cycle is internal. Our model extends and generalizes this methodology to simulate communication.

Our network is implemented using the encoding-decoding operations of an autoencoder, which ultimately converge to attractors in its final version [28]. The key difference between our classifier and approaches that utilize denoising autoencoders [2,3] lies in the iterative nature of the encoding and decoding operations, which leads to convergence to attractors.

Our model is employed to model the semiotic properties of person-object perception and person-to-person communication. Furthermore, it can be utilized in computer vision classification tasks. By leveraging our observed-to-seen model, we have created an image classifier that exhibits high interpretability and performs well with small training datasets.

In [11], attractors were utilized for classification in the field of speech recognition. In [4], the attractor-based classifier is employed to estimate the normalized entropy [34] of the probability vector. This approach is used

to detect novel sceneries, such as out-of-distribution or anomaly samples, rather than specifically focusing on the classification task.

Our classifier is stochastic and builds upon the vanilla version, which is non-stochastic. The vanilla version represents an input sample as a single convergent point in the image space, resulting from encoder and decoder operations. In contrast, in [11], a sample is represented as a series of convergence points in the latent space, obtained through MC dropout.

Modern networks, including those employed for classification tasks, commonly offer confidence values alongside the predicted output class. These confidence values can be obtained through various means, such as utilizing historical information or running the network multiple times, such as in ensemble approaches. In our approach, our focus lies in enriching the attractor-based representation by introducing minor perturbations during the convergence process, specifically in the image domain. Our main objective is to enhance the expressiveness of the attractor-based representation rather than estimating confidence.

Specifically, in our stochastic classifier, an input sample is represented by a set of attractors that are in close proximity to the sample, thereby enhancing the informativeness of the attractor-based representation. The construction of the attractor sets involves randomized iterative alternations of the samples in the image domain. Referring to [11], the alternation of samples during recursive autoencoder operations is achieved using Monte Carlo (MC) dropout. Notably, a meaningful distinction arises between our attractor representation and dropout [11]. The dropout mechanism generates outputs that represent known samples with similar representations and unknown ones with dissimilar representations. However, our representation typically assigns different attractors to all input samples, including those used in training, thereby enhancing the informativeness of the attractor-based representation.

Technically, our representation may resemble the SIFT approach [20]. There, instead of considering a specific pixel, sift considers the neighboring area of the pixel, known as the 'vicinity', where the histogram representations for gradient directions are calculated. In our approach the 'histogram bins' are comprised of the results of convergence of the algorithm and are not predefined.

Our work has some common ground with RNN networks. In both, an internal state is preserved and is used and updated when new inputs are being processed. In this light, our model can be examined as a few RNN networks, each representing one person, that communicate with each other. In classical RNN networks, the internal state can receive any value (with

some implementation detail limitations). On the other hand, our model attempt to preserve its internal model within a certain 'pre-defined' set.

Our model introduces innovative techniques for analyzing and interpreting visual information in a social context. By integrating person-to-person communication cues and object perception capabilities, our approach aims to model social perception of visual objects. In the subsequent sections, we will provide a detailed description of our model and discuss the experimental results that demonstrate its effectiveness.

3 Modeling Person-Person and Person-Object Communication using Semiotic Networks

In this section we introduce the Concious Neural Network (CONN) for modeling communication between persons perceiving visual images. Consider two persons P_1 and P_2 (Fig. 1(A)). The first person tends to see in all input images the cats, the second the dogs. Assume the persons perceive the images iteratively: the P_1 converts an observed input image Im to an internal image with some features of the cat, refereed as 'seen' image for the observed, and then continues iteratively recognize 'catness' in the seen image. Similarly, the person P_2 tends to see 'dogness' in the perceived images. This is expressed as

$$Im = obs_1 \xrightarrow{O2S_P} seen_1 = obs_2 \xrightarrow{O2S_P} seen_2 = obs_3 \xrightarrow{O2S_P} \dots, \quad (1)$$

where the seen images obtained at each iteration became the observed for the next iteration, and $P \in \{P_1, P_2\}$.

The persons communicate, representing to each other their seen images, obtained from the input images after a certain number of iterations. In general, the transmitted representations do not have to be of image modality (they may be, for example, textual descriptions). Meanwhile, we confine ourselves to the case where these representations are themselves the internal seen images.

The introduced scheme is a particular case of a 'DoWheel' scheme, where the images of Eq. 1 form the person aligned stream (PAS) associated with the persons [17].

Our scheme allows to model perception of a visual object by a person as a private case of person to person communication. The Fig. 2 illustrates perception of an object (an apple) by a person. The $O2S$ transformation associated with an apple does not depend on the input and always returns 'a

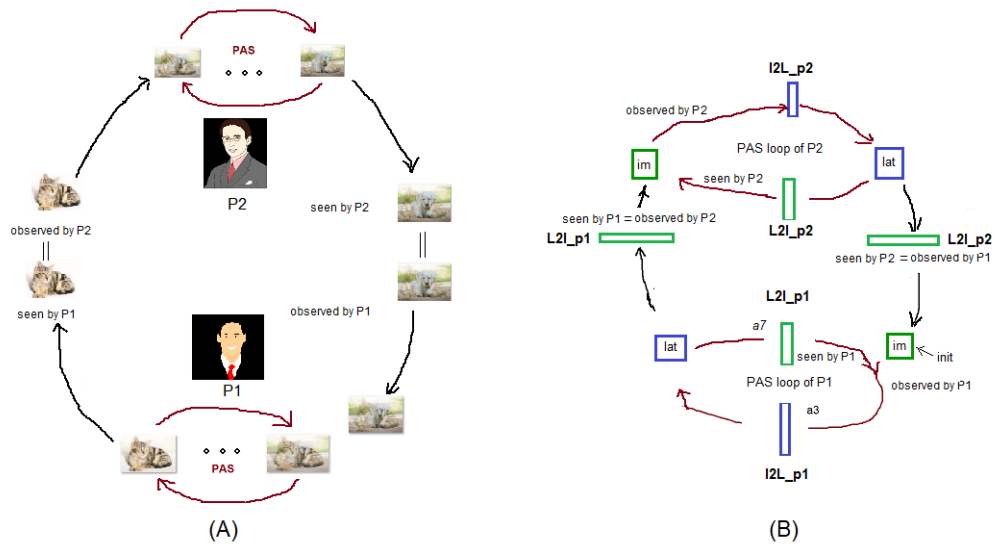


Figure 1: (A) Person-to-person CONN. (B) Person-to-person CONN with observed-to-seen transformation implemented as composition of encoder and decoder operations shown in blue and green respectively.

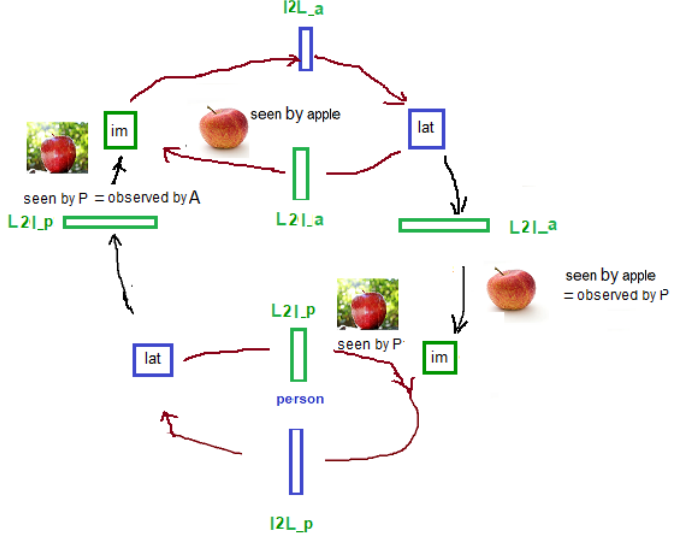


Figure 2: Perception of an object by the person may be treated as a private case of the person to person communication.

raw' (non-personalized) image of the apple. The image becomes the observed by the person and is further personalized in $obs \rightarrow seen$ transformations.

To reflect uncertainty involved in human perception [12,36] we add some randomness to Eq. 2 as described in the following section.

4 Implementation of Semiotics Networks Using Convolutional Autoencoder

In general, the $obs \rightarrow seen$ person-dependent transformation of Eq. 1 may be modeled in different ways. We model this transition using enc and dec operations of convolution autoencoders performing transformations from the image space to a latent space and back:

$$obs \rightarrow seen : obs \xrightarrow{enc} enc(obs) \xrightarrow{dec} seen = dec(enc(obs)). \quad (2)$$

Note that both 'observed' and 'seen' representation are of the object modality and not in latent space. Transition from 'observed' to 'seen' is through latent based representations.

Using these operations we construct a conscious neural network for person-to-person communication. The network is illustrated at Fig.1 (B), its work

is described by Algorithm 1.

Algorithm 1 A concious neural network for person-to-person communication of k transactions.

Input: an image Im_1 which is related to person P_1 (marked by 'init' in Fig. 1 (B))

Output: A sequence of transaction images $Im_1, Im_2, \dots, Im_k, \dots$

1. Set $iter = 1$;
2. Set $person_id = 1$;
3. While $iter \leq n_iters$ do:
 - 3.1. Use $person_id$ parameters ($nsteps_{person_id}$);
 - 3.2. Perform $nsteps_{person_id}$ encoding/decoding iterations of Eq. 2 on Im_{iter} to receive the image representation (current Im).
 - 3.3. Decode the previous encoding result lat (current $Im = dec(lat)$) to receive Im_{iter+1} (Im_{iter+1} = current Im after this operation).
 - 3.4. Increase $iter$ by 1 and change $person_id$ to other $person_id$
 - 3.5. Send Im_{iter} to the updated person and return to step 2

4.1 Perception of an object by one person: attractors

In this subsection, following in Sect.,3, the perception of an object by a person will be modeled as a specific case of person-to-person communication. Furthermore, we model the transformation from 'observed' to 'seen' as a sequence of encoder/decoder operations of an autoencoder. This will lead us to the fixed point property [28], which will be essential in our modeling of the semiotics of human perception in Sect.,6.

As shown in Sect. 3, the perception of an object by a person can be considered as a specific case of person-to-person communication. When modeling the perception of an object, each internal communication cycle of images associated with a person begins with the same observed image Im (Fig. 2). This cycle is described as follows:

$$Im = obs_1 \xrightarrow{O2S_P} seen_1 = obs_2 \xrightarrow{O2S_P} seen_2 = obs_3 \xrightarrow{O2S_P} \dots \xrightarrow{O2S_P} seen_n, \quad (3)$$

where $n = nsteps$ represents the length of the internal communication loop of the person.

Using the notation of Eq. 2 we may write this sequence as:

$$Im \rightarrow dec(enc(Im)) \rightarrow, \dots \rightarrow [dec(enc)]^n(Im), \quad (4)$$

where $[dec(enc)]^n$ denotes n compositions of $dec(enc)$ function.

The process takes an input image Im , encodes it into the latent space using $enc(Im)$, and then decodes it back to the image space. This encoding/decoding procedure is repeated n times, resulting in an image representation in the original modality. As n approaches infinity, this sequence has been studied in [28], where the phenomenon of attractors has been identified. It has been empirically shown that for overparameterized autoencoders, as n approaches infinity, the sequence described in Eq. 4 converges to an attractor. We have also observed similar phenomena for autoencoders that are not overparameterized, where the CONNs map input examples to attractors (see Sect.7).

For an input image Im be an input image we call the final representation of Im in the image space

$$\hat{x} = \lim_{n \rightarrow \infty} [dec(enc)]^n(Im), \quad (5)$$

if such limit exist, the *percept image* of Im .

From [28] above follows that there is empirical evidence that the percept image for overparameterized autoencoder is attractor.

One can observe that for the percept image \hat{x} , there holds the fixed point property:

$$dec(enc)(\hat{x}) = \hat{x}. \quad (6)$$

This equation indicates that applying the encoding and decoding operations to the percept image results in the same image.

We will use this fixed point property of the percept image in Sect. 6.1 where semiotic properties of the person-object relationship are studied.

4.2 Perception of an object by two persons: bipartite orbits

In this subsection, we will delve into inter-person communication. We will study the asymptotic properties of the image sequence exchanged between individuals in our CONN model (Sect. 3). These properties will play an important role in our subsequent exploration of the semiotic properties of interpersonal communication in Sect.6.2.

In contrast to the previous subsection, our exposition will not be limited to sequences implemented through encoder/decoder operations. Instead, it is applicable to sequences defined in terms of general metric spaces. The representation of the image sequence transmitted between individuals in the person-to-person CONN, which is implemented using encoder/decoder operations, can be found in Appendix A.

What periodicity is being referred to? One may assume that the sequence of the images 'perceived' by the person as reflected in Eq. 1 of our CONN model converged to 'attractors'. For example, for a 'dog-like' person, the sequence is converged to a dog image. However, when more than one person is involved, this assumption may not hold anymore for the whole sequence of intertransmitted images, because there is no guarantee that both persons share the same 'attractors'. For example, if one is a 'dog-like' person (i.e., the attractors are comprised of dogs images only) and the other is a 'cat-like' person, then a joint attractor is of a low choice. A 'dog-like' person is unlikely 'to see' a cat image and vice versa for the 'cat-like' person.

Although the sequence of intertransmitted images, generally speaking, does not converge as a sequence of elements, our empirical findings, together with theoretical endorsement, indicate that this is an asymptotically periodic sequence [14], as we shall see later.

Specifically, we will identify two types of periodicity in the sequence of transmitted images between the persons. Both types are observed when the external communication parameter of the algorithm (the number of information exchanges between the persons) tends to infinity. The difference lies in whether the internal communication parameters (the number of observed/seen transformations in Eq. 1) also tend to infinity. These two types of periodicity are studied in Sects. 4.2.1 and 4.2.2, respectively.

From a mathematical perspective, we will examine sequences consisting of compositions of functions F_1 and F_2 , applied alternately to the elements of the sequence. The only requirement for F_1 and F_2 is that they are functions operating in metric spaces.

4.2.1 Bipartite orbits of the first type

In the previous section (4.1), attractors were considered, as modeling perception of an object by one person. Interestingly, when human *communication* is simulated, an asymptotically periodic sequence of inter-person transmitted images had been identified. We denote this property as convergence to bipartite orbits.

Formally, let F_{P_1} and F_{P_2} be two continuous functions $X \rightarrow X$ where X

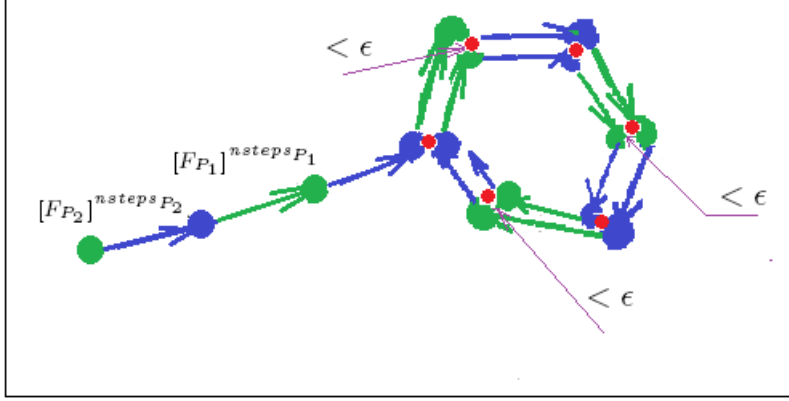


Figure 3: Illustration of bipartite orbit for (A) The bipartite orbit of the first type, for n_{iter} tending to infinity (Definition 4.1), (B) The bipartite orbit of the second type, for n_{iter} , n_{steps_1} , and n_{steps_2} tending to infinity (Definition 4.4). Elements of the bipartite orbit are shown in red. .

is a metric space and $Im \in X$ to be a initial point ('an image'). Consider a sequence $W(Im)$ starting with Im and consisting of subsequent application of n_{steps_1} times of F_{P_1} , then n_{steps_2} times of F_{P_2} , then n_{steps_1} times of F_{P_1} etc., where n_{steps_1} and n_{steps_2} are given numbers (representing the internal number of steps for convergence of Persons 1 and 2). If we denote

$$\begin{aligned}
 S_{1,P_1} &= Im, F_{P_1}(Im), \dots, [F_{P_1}]^{n_{steps_1}}(Im); \\
 T_{1,P_1} &= [F_{P_1}]^{n_{steps_1}}(Im); \\
 S_{2,P_2} &= T_{1,P_1} F_{P_2}(T_{1,P_1}), \dots, [F_{P_2}]^{n_{steps_2}}(T_{1,P_1}); \\
 T_{2,P_2} &= [F_{P_2}]^{n_{steps_2}}(T_{1,P_1}); \\
 S_{3,P_1} &= T_{2,P_2} F_{P_1}(T_{2,P_2}), \dots, [F_{P_1}]^{n_{steps_1}}(T_{2,P_2}); \\
 T_{3,P_1} &= [F_{P_1}]^{n_{steps_1}}(T_{2,P_2}); \dots
 \end{aligned} \tag{7}$$

then one may write

$$W(Im) = S_{1,P_1}, S_{2,P_2}, S_{3,P_1}, \dots, S_{n_{iter},P_{n_{iter}}}, \dots \tag{8}$$

¹

¹This representation is identical to Eq. 33, but there, W was defined in terms of encoding and decoding operations.

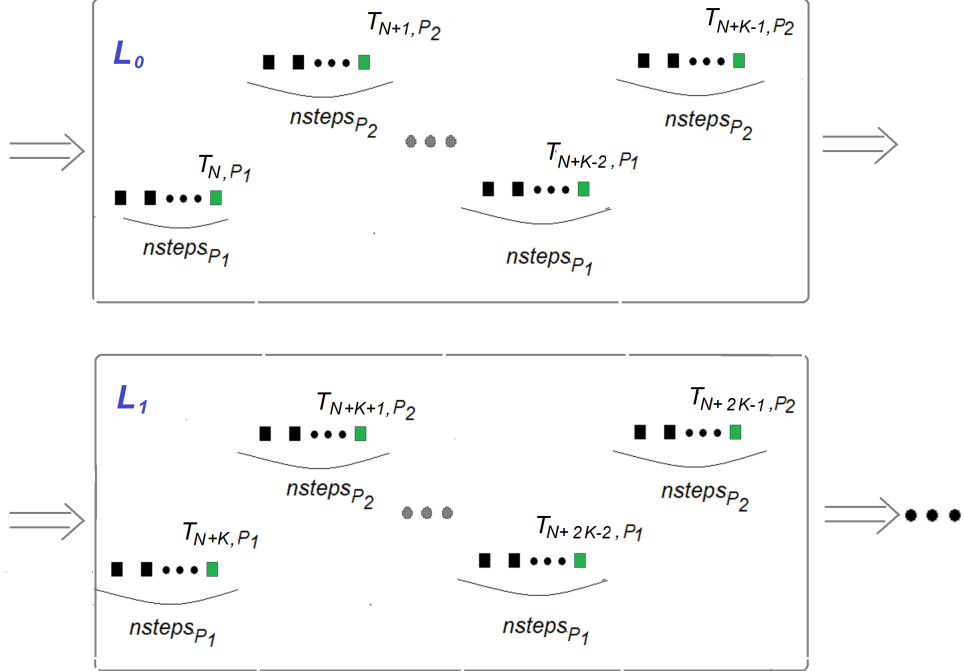


Figure 4: Illustration of bipartite convergence of the first type (Definition 4.1). A bipartite convergent sequence U (Eq. 35) is shown in green 'within' sequence W (Eq. 8). Starting from the $N(\epsilon)$ -th iteration sequence U may be partitioned by subsequences $U = L_0, L_1, \dots$ such that for every $m_1, m_2 \geq 0$ $d_{SAD}(L_{m_1} - L_{m_2}) < \epsilon$.

Now focus on the 'final' internal elements $T_{1,P_1}, T_{2,P_2}, T_{3,P_1} \dots$ in this representation (see Eq. 7). These elements represent the final image of each person, that is later sent to the other person. They are marked in green in Fig. 4. These elements comprise a sub-sequence U of W :

$$U(Im, nsteps_1, nsteps_2) = Im \xrightarrow{[F_{P_1}]^{nsteps_1}} T_{1,P_1} \xrightarrow{[F_{P_2}]^{nsteps_2}} T_{2,P_2} \xrightarrow{[F_{P_1}]^{nsteps_1}} T_{3,P_1} \xrightarrow{[F_{P_2}]^{nsteps_2}} T_{4,P_2} \xrightarrow{[F_{P_1}]^{nsteps_1}} \dots \quad (9)$$

Denote

$$F_1 = [F_{P_1}]^{nsteps_1}, F_2 = [F_{P_2}]^{nsteps_2}. \quad (10)$$

For any $K > 0$ one may partition $1 + (n+1)*K$ members of the sequence by Im following the matrix of $(n+1)$ rows and K columns (see Appendix B).

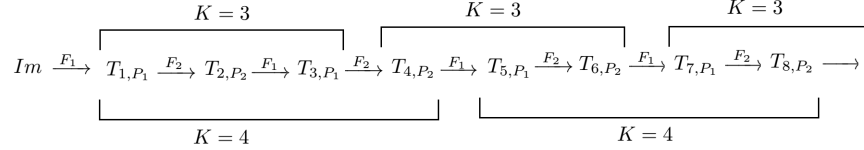


Figure 5: Partitioning U by segments of $K = 3$ and $K = 4$.

Like this, for any $K > 0$ we may partition the whole sequence by Im following subsequent segments of length K , see Fig. 5. Our convergence will be defined by way of columns of the matrix whose lines are the K -length segments of such partitioning.

Specifically, for any $K > 0$ the sequence may be written as follows:

$$\begin{aligned}
 U(Im, nsteps_1, nsteps_2) = Im &\xrightarrow{F_1} \\
 T_{1+0 \cdot K, P_1} &\xrightarrow{F_2} T_{1+0 \cdot K+1, P_2} \xrightarrow{F_1} \dots \xrightarrow{F_2} T_{1+0 \cdot K+K-1, P_2} \xrightarrow{F_1} \\
 T_{1+1 \cdot K, P_1} &\xrightarrow{F_2} T_{1+1 \cdot K+1, P_2} \xrightarrow{F_1} \dots \xrightarrow{F_2} T_{1+1 \cdot K+K-1, P_2} \xrightarrow{F_1} \\
 &\dots \\
 T_{1+n \cdot K, P_1} &\xrightarrow{F_2} T_{1+n \cdot K+1, P_2} \xrightarrow{F_1} \dots \xrightarrow{F_2} T_{1+n \cdot K+K-1, P_2} \xrightarrow{F_1} \\
 &\dots
 \end{aligned} \tag{11}$$

For $j = 0, \dots, K - 1$ the j 's column of this representation is written as

$$C_j(nsteps_1, nsteps_2) = \begin{pmatrix} T_{1+0 \cdot K+j, P_{i(j+1)}} \\ T_{1+1 \cdot K+j, P_{i(j+1)}} \\ \dots \\ T_{1+n \cdot K+j, P_{i(j+1)}} \\ \dots \end{pmatrix}, \tag{12}$$

where $i()$ is defined in Eq. 31 and the column comprises the sequence indexed by n .

Definition 4.1 (Bipartite convergence of the first type to orbit). *A sequence $U(Im, nsteps_1, nsteps_2)$ is a bipartite convergent sequence of the first type converging to orbit $(b_j \mid j = 0, \dots, K - 1)$ if for a certain $K > 0$ and for every $j = 0, \dots, K - 1$ column $C_j(nsteps_1, nsteps_2)$ as a sequence converges to b_j at n tending to infinity.*

The definition is illustrated at Fig 3. At Fig 4 a bipartite convergent sequence U is shown in green 'within' the sequence W (Eq. 8).

The following statement is obvious.

Statement 4.2. *A sequence $U = U(Im, nsteps_1, nsteps_2)$ is a bipartite sequence of the first type if and only if it is an asymptotically K -periodic sequence?? w.r.t. index iter (Eq. 8). In this case the sequence comprising the period of U is the bipartite orbit of U . \square*

For a bipartite sequence starting with an image Im alternation of $nsteps$ parameters typically leads to alternation of the period, as illustrated in SI Text A.

Under what conditions a sequence $U(Im, nsteps_1, nsteps_2)$ is a bipartite convergent sequence of the first type? Although the existence of such orbits was not formally proven, in our experiments with the autoencoder generated images (we did not specify that the autoencoder is overparameterized), we empirically observed convergence to the bipartite orbits for every initial Im , $nsteps_1$, and $nsteps_2$ (Sect. 7). In addition, we developed a simplified computational model for simulating inter-person communication (see SI Text B). The running of the model consistently demonstrates convergence to what can be referred to as the first type orbit of the simplified model.

For a bipartite sequence starting with an image Im alternation of $nsteps$ parameters typically leads to alternation of the period length, as illustrated in SI Text A.

For the first type bipartite orbits there hold the following statement.

Statement 4.3. *The elements of bipartite orbits $(b_0, b_1, \dots, b_{K-1})$ of the first type satisfy the following properties:*

1. *They form a loop with respect to alternating F_1 , F_2 operations:*

$$b_0 \xrightarrow{F_2} b_1 \xrightarrow{F_1} \dots \xrightarrow{F_2} b_{K-1} \xrightarrow{F_1} b_0, \quad (13)$$

where F_1 , F_2 are defined as in Eq. 10:

$$\begin{aligned} F_1 &= [F_{P_1}]^{nsteps_1}, \\ F_2 &= [F_{P_2}]^{nsteps_2}. \end{aligned}$$

2. *These elements are also alternating fixed points of functions G_1 , G_2 :*

$$\begin{aligned} G_1(b_h) &= b_h, \text{ for even } h, \\ G_2(b_h) &= b_h, \text{ for odd } h. \end{aligned} \quad (14)$$

where

$$\begin{aligned} G_1 &= [F_1 \cdot F_2]^{K/2}, \\ G_2 &= [F_2 \cdot F_1]^{K/2}. \end{aligned} \tag{15}$$

Proof. See C. □

It should be noted that the elements comprising the bipartite orbits of the first type are not necessarily the attractors of F_1 or F_2 . This is due to 'non-deep' character of the intra-person communication (the $nsteps_1, nsteps_2$ are not tending to infinity).

We call G_1 , and G_2 the *personalized operators of the seen in the dialog* and consider their interpretation in Sect.6.2 where the semiotics aspects of the person to person communication will be studied.

4.2.2 Bipartite orbits of the second type

In this subsection, similar to the previous one, we will explore the periodic properties of the converging sequences, which will be further interpreted from a semiotic perspective in Sect. 6.2.

Specifically, we will consider the behavior of the 'internal' person parameters, $nsteps_1$ and $nsteps_2$, as they tend towards infinity in $U(Im, nsteps_1, nsteps_2)$, as defined in Eq. 9. These parameters represent the steps involved in converging towards the 'innate representations'. These representations, implemented in our model using autoencoders as described in Sect.,4, are characterized as fixed points.)

Additionally, as mentioned earlier, our assumption regarding F_1 and F_2 is that they are functions operating within metric spaces.

The convergence of the sequence $U(Im, nsteps_1, nsteps_2)$, as discussed in Sect. 4.2.1, describes its behavior as *iter* of Algorithm 1 (or equivalently, Eq. 8) tends to infinity. Now, let us consider the behavior of U when both $nsteps_1$ and $nsteps_2$ also tend to infinity.

Definition 4.4 (Bipartite convergence of the second type to orbit). *A sequence $U(Im, nsteps_1, nsteps_2)$ is a bipartite convergent sequence of the second type converging to orbit $(b_j \mid j = 0, \dots, K - 1)$ if for a certain $K > 0$ and for every $j = 0, \dots, K - 1$ column $C_j(nsteps_1, nsteps_2)$ (Eq.12) as a sequence converges to b_j at $n, nsteps_1$, and $nsteps_2$ tending to infinity.*

Likewise the convergence of the first type, the definition stipulates that the behavior of U is like the shown at Fig. 3.

Like Statement 4.2 the following statement is obvious.

Statement 4.5. *A sequence $U = U(Im, nsteps_1, nsteps_2)$ is a bipartite sequence of the second type if and only if it is an asymptotically K -periodic sequence w.r.t. $nsteps_1$, $nsteps_2$, and $iter$. In these cases the sequence comprising the period of U is the bipartite orbit of U . \square*

In our experiments we empirically observed convergence to the bipartite orbits of the second type for every initial Im . (Sect. 7). The same phenomena was observed for a simplified model of the inter-person communication (see SI Text B).

The following questions arise.

1. Under what conditions U is as a bipartite sequence of the second type?
2. What are the properties of the bipartite sequence of the second type?

The following statement answers to these questions under certain natural conditions.

Statement 4.6. *If both F_{P_1} , F_{P_2} satisfy certain natural conditions (See E.1), then $U(Im, nsteps_1, nsteps_2)$ a bipartite convergent sequence of the second type converging to orbit $B = (b_0, b_1, \dots, b_{K-1})$ of the second type. There are hold the following properties.*

1. *B is comprised of alternating attractors of F_{P_1} , F_{P_2} (see Eq. 34).*

In particular there hold the fixed point relations:

$$\begin{aligned} F_{P_1}(b_h) &= b_h, \text{ for odd } h, \\ F_{P_2}(b_h) &= b_h, \text{ for even } h, \end{aligned} \quad (16)$$

2. *They form a loop with respect to alternating \widehat{F}_1 , \widehat{F}_2 operations:*

$$b_0 \xrightarrow{\widehat{F}_2} b_1 \xrightarrow{\widehat{F}_1} \dots \xrightarrow{\widehat{F}_2} b_{K-1} \xrightarrow{\widehat{F}_1} b_0, \quad (17)$$

where

$$\widehat{F}_i(Im) = \lim_{n \rightarrow \infty} [F_{P_i}]^n(Im); \quad (18)$$

3. *These elements are also alternating fixed points of functions \widehat{G}_1 , \widehat{G}_2 :*

$$\begin{aligned} \widehat{G}_1(b_h) &= b_h, \text{ for even } h, \\ \widehat{G}_2(b_h) &= b_h, \text{ for odd } h, \end{aligned} \quad (19)$$

where

$$\begin{aligned} \widehat{G}_1 &= [\widehat{F}_1 \cdot \widehat{F}_2]^{K/2}, \\ \widehat{G}_2 &= [\widehat{F}_2 \cdot \widehat{F}_1]^{K/2}. \end{aligned} \quad (20)$$

Table 1: Properties of Bipartite Orbits

#	Property	Type of bipartite orbit		References
		The First	The Second	
1	Infinity limit parameters	$nsteps_1$, $nsteps_2$	$niter$, $nsteps_1$, $nsteps_2$	
2	Semiotics interpretation			Sect. 6
3	Attractors of F_{P_1}, F_{P_2}	Typically not	Yes	Eq. 34, Eq. 16
4	Alternating cyclic transition functions	F_1, F_2	$\widehat{F_1}, \widehat{F_2}$	Eq. 10, Eq. 13, Eq. 17
5	Fixed points identities functions	G_1, G_2	$\widehat{G_1}, \widehat{G_2}$	Eq. 15, Eq. 14, Eq. 19
6	Algebraic operation for theme loop formation	FM	\widehat{FM}	SI Text C
7	Validation of existence	Observed experimentally	Proven under certain natural conditions. Also, observed experimentally.	Statement 4.6

Proof. See E.1. \square

\square

One may that Eqs. 17 and 19 are the counterparts of Eqs. 13 and 14 from Sect. 4.2.1 respectively. The essential difference between the two types of the orbits is that the orbits of the first type are comprised of attractors. The semiotics aspects of the both types of the orbits are considered in Sect. 6. In particular, we demonstrate that the b_h values with even (resp. odd) values of h correspond to what person P_1 (resp. P_2) is aware of as seen in the dialogue. These elements are represented by the red (resp. blue) portions in Eq. 17.

In SI Text C we study monocular algebras associated with the bipartite orbits of the both types.

Finally, Table 1 summarizes the properties of bipartite orbits.

5 Attractors-based classifier

In the previous sections, we introduced a model for person-to-person communication that relies on observed-to-seen transformations that converge to attractors. This model allows us to describe several semiotic phenomena related to Person-Object and Person-Person communication (see Section 6). In this section, we demonstrate that the model can also be applied to classical computer vision tasks, such as classification.

Our objective is to investigate whether our person-object communication model, which is based on attractors [28], can be applied to classification tasks. We introduce an attractor-based classifier network and demonstrate its effectiveness for tasks with small training datasets. Our classifier provides interpretability, enabling us to understand how the network perceives the input image as a whole. However, the effectiveness and interpretability come at a cost of longer inference time, as input samples take longer to converge to attractors.

In the following subsections, we describe two types of attractor-based classifiers: vanilla and stochastic. While the vanilla classifier is more suitable for representing the semiotic properties of communication (see Sect. 6), the stochastic variant demonstrates superior performance properties. Specifically, the stochastic attractor-based classifier shows improved classification performance, making it a more suitable choice for classification tasks with small training datasets.

5.1 Vanilla classifier

In this subsection, we introduce the conversion of an image classifier M into a vanilla CONN classifier. This conversion can be viewed as the addition of a new 'perceptual' layer that precedes the input of M .

Overall, our approach involves applying the same transformation to the labeled sets of training and test examples, TR and TE , respectively. This transformation converts these sets into sets ATR and ATE . These transformed sets consist of attractors and are used as the new training and test sets for the classifier.

First consider a mapping of image samples to attractors using an autoencoder. In [28], it was empirically demonstrated that, for an overparameterized autoencoder, for an arbitrary image Im , the sequence composed of encoder and decoder operations of the autoencoder typically converges to the input image stored as an attractor: The attractor for an overparameter-

ized autoencoder is defined as:

$$\widehat{F}(Im) = \lim_{n \rightarrow \infty} [dec(enc)]^n(Im). \quad (21)$$

Given a training set TR , we first train an overparameterized autoencoder A to memorize TR (without using the labels of TR). We then construct a new training set comprised of attractors:

$$ATR = \{\widehat{F}(Im) \mid Im \in TR\}$$

We assign the same labels to the images $\widehat{F}(Im)$ as to Im . Due to memorization, ATR is identical to TR . (In the following subsection, we define the stochastic classifier, which follows the general CONN classifiers framework. Notably, in the stochastic classifier, ATR differs from TR .) Set ATR is used to train the benchmark classifier M .

During inference, test data samples Im from TE are converged to attractors (using Eq. 21), resulting in a set ATE consisting of attractors from ATR , including potentially spurious attractors [28]. Finally, the elements of ATE are passed to the classifier M for prediction.

In Fig. 6 (A), we can see a vanilla classifier C comprising of an overparameterized autoencoder A and a benchmark classifier M . For the vanilla classifier, transformation F refers to the conversion to attractors, as defined in Eq. 21.

The ability of autoencoder A to accurately preserve the original information in the input samples has an essential impact on the classifier's performance. In particular, our goal is for images from the training data to converge to an attractor $a(Im)$, such that $a(Im)$ is similar to Im . Therefore, for higher performance of the classifier C , we require a lower reconstruction error of autoencoder A on the training data. Currently, the memorization of training data is demonstrated for autoencoders trained on data sets consisting of up to several hundred examples [28]. Due to this factor, the current usage of the CONN-based classifier is restricted to situations where the available training data is limited in size.

Experimental results for the vanilla attractor-based classifier are presented in Sect. 7.

In our approach, the mapping of input samples to attractors can be categorized as prototype-based methods [1]. These methods classify new data points by comparing them to a set of existing prototypes or examples that represent the classes in the data.

The suggested approaches demonstrate that the performance of prototype-based methods can be improved by exploring similarities between prototypes. This approach has been used, for example, in [32] for the person

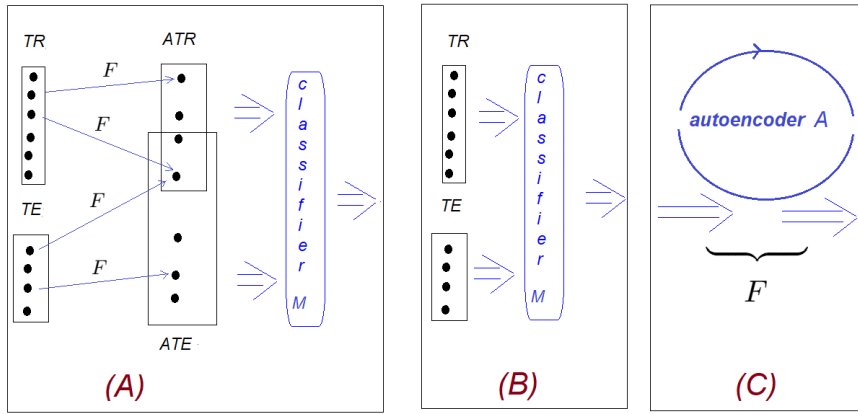


Figure 6: (A): The attractor-based classifier C is constructed by first converting the training dataset TR and test dataset TE samples into new training and test datasets ATR and ATE , respectively. This conversion takes place prior to the training of the benchmark classifier M , which is subsequently trained on the ATR dataset and tested on the ATE dataset. The conversion is achieved through the application of transformation F , shown in (C). (B): The benchmark classifier M is used for comparison with the attractor-based classifier (refer to Sect. 7). (C): For the vanilla classifier (refer to Sect. 5.1), the transformation F denotes the transformation \hat{F} to attractor (Eq. 21). For the stochastic classifier (refer to Sect. 5.2), F denotes the transformation F^* to the averaged randomized assemble of attractors (Eq. 22).

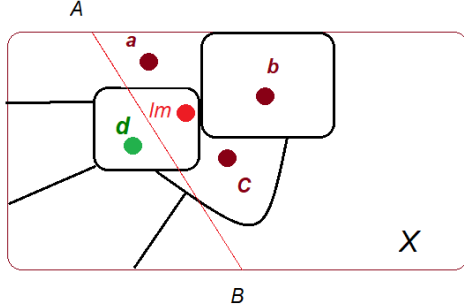


Figure 7: Comparison of image representation by attractors in vanilla and stochastic attractor-based classifiers in an image space X . The a, b, c (respectively d) are memorized training examples for the first (respectively second) class, shown in the basins [28] of the attractors. An image Im is represented in the vanilla classifier by attractor d . An attractor assembly $SA(x)$ obtained by randomized transitions to attractors starting with Im consists of multiple instances of a, b, c , and d , providing a more informative representation of x by attractors of different classes. The image space X is divided into two classes by the decision boundary (A, B).

re-identification problem. In the case of the attractor-based classifier, we explore this approach in a stochastic classifier considered in the following subsection.

5.2 Stochastic classifier

The vanilla classifier considered in the previous section is based on the representation of an input sample Im by a single attractor (Eq. 21). However, this representation may not be sufficiently informative.

This is illustrated in Fig. 7, which shows a two-class classification problem. An image space X is divided into two classes by the decision boundary (A, B). For a vanilla attractor-based classifier C a test sample Im , is represented by attractor $\hat{F}(x) = d$ (Eq. 21). A vanilla classifier C will map an input Im to d following application of M to d . Thus, assuming the benchmark classifier M correctly classifies d , vanilla classifier C will mistakenly classify Im .

Our objective is to enhance the informativeness of the attractor-based representation. Instead of representing Im solely by a sequence of elements converging to an attractor, as done in the vanilla classifier, we introduce

$J > 0$ sequences that start with Im and converge to attractors. These sequences are constructed in a similar manner as described in Eq. 21, but they also incorporate random augmentations. As a result, we obtain an ensemble of J attractors, which may contain repetitions, that are similar to Im . This ensemble offers a more comprehensive description of Im through the utilization of attractors, as demonstrated in Fig. 7. Additionally, we derive the final attractor representation $F^*(Im)$ by averaging the ensemble in the image domain (see below).

Likewise the vanilla classifier, the stochastic classifier is depicted in Fig. 6 (A). The difference between the two classifiers is that the transformation F in the present case converts to the averaged randomized collection of attractors, as defined further in Eq. 22.

Accordingly, for overparameterized autoencoder and an input image Im define an Averaged Randomized Assemble of Attractors

$$F^*(Im) = \frac{1}{J} \sum_{j=1}^J a_j, \quad (22)$$

where assemble

$$\{a_j \mid j = 1, \dots, J\}$$

is comprised of J attractors

$$a_j = \lim_{i \rightarrow \infty} x_{i,j}, \quad (23)$$

where

$$x_{0,j} = Im,$$

and

$$x_{i+1,j} = dec(enc(\tau_j(x_{i,j}, \gamma_i))) \quad (24)$$

for $i \geq 0$.

The term $\tau_j(x_{i,j}, \gamma_i)$ represents a sampling of random augmentation of the image $x_{i,j}$, where the magnitude of augmentation is denoted by γ_i . The specific augmentation applied is dependent on the index j .

When $\gamma = 0$, it signifies that no augmentation is applied to the image. On the other hand, when $\gamma = 1$, it indicates the maximum possible level of augmentation. We assign the value of γ_i using the formula:

$$\gamma_i = \beta^{\frac{1}{i+1}}, \quad (25)$$

where the parameter $\beta > 1$ controls the relaxation of the augmentation amplitude as i increases.

As discussed above, the stochastic classifier was designed to explore more informative image representations compared to the vanilla classifier. Let's revisit Fig. 7 and explore the operational differences between these two types of classifiers. For a given image Im from the figure, the vanilla classifier behaves similarly to a one-nearest neighbor approach. It converts Im to the 'nearest' memorized training example d , which is then typically assigned the ground truth label by the application of M . The stochastic classifier, on the other hand, generalizes the vanilla classifier by representing Im through a combination of several 'nearest' training examples following the application of the benchmark classifier, resulting in more accurate classification compared to the vanilla classifier.

Intuitively, when adding new training examples, the 'density' of the attractors around the image Im increases, and the representation of Im improves. However, as we continue to add more and more attractors, the additional representations become less and less significant in improving the overall representation of Im . The improvements start to relax because the additional attractors start capturing finer and finer details that might not have a significant impact on the overall representation.

Our experimental results in Sect. 7.2 demonstrate that the stochastic classifier significantly outperforms the vanilla one. These also demonstrate that as we add more training examples, the improvement in performance of the stochastic classifier compared to the vanilla one starts to level off, indicating that the stochastic classifier is already efficiently utilizing the available training data.

The key takeaway from our experimental results in Sect. 7.2 is that the stochastic classifier consistently outperforms the benchmark classifier on small training databases used in the experiments. Specifically, it exhibits significant superiority in general over the benchmark when the MNIST training database contains less than 10 samples. However, as the number of training samples increases, the benchmark classifier starts to slightly outperform the stochastic one. This behavior can be attributed to the saturation of improvement in the stochastic classifier's performance with increasing training examples. These results are further illustrated in Fig. 19.

It is worth noting that although the stochastic CONN classifier explores augmentations, the approach itself is not an augmentation of the training examples. In fact, the number of training examples in the stochastic classifier remains the same as in the vanilla version.

Technically, our representation may resemble the SIFT approach [20] where the histogram representations for gradient directions are calculated, but in our approach the histogram bins are comprised of the results of con-

vergence of the algorithm and are not predefined.

The transformation of $\widehat{F}(Im)$ into an attractor (Eq. 21) represents the final form of the observed transformations (Eq. 1). Therefore, it is natural to refer to it as the *seen* transformation of an image Im that is *observed* by a vanilla classifier C_V :

$$seen_{C_V}(Im) = \widehat{F}(Im). \quad (26)$$

Similarly, we will refer to $F^*(Im)$ (Eq. 22) as the *seen* transformation by a stochastic classifier C_S :

$$seen_{C_S}(Im) = F^*(Im). \quad (27)$$

In the stochastic CONN classifier, we perform a series of converging sequences, where each sequence is terminated by an attractor. The attractors in the series may vary, but they demonstrate consistency throughout the series. For example, the set of attractors obtained during descents [1:50] in the series is typically equal to the attractor set obtained during descents [50:100]. Additionally, the terminating elements (attractors) are predefined, meaning they are determined solely by the training examples.

This allows us to view the stochastic CONN classifier from the perspective of visual perception, particularly in relation to multistable perception. Multistable perception, as demonstrated by the Rubin’s face-vase illusion and similar phenomena [13], involves the perception of different patterns. These patterns are typically consistent and predefined for individuals over time, although different individuals may perceive different patterns. For instance, in the Rubin’s vase/face illusion, the perceived patterns typically consist of either a vase or a face.

In this regard, the stochastic CONN classifier mimics the properties of consistency and predefinency observed in human multistable perception. In Section 8, we will consider how these properties are related to the awareness of CONN networks.

6 Semiotics Interpretation of the model

In this section, we will explore how our model describes the semiotic phenomena of human perception. We begin by discussing the perception of a visual object by a single person, followed by an exploration of two-person communication.

6.1 Perception of a visual object by a person

The goal of this section is to specify the semiotic relations that describe human perception of visual objects and demonstrate how the communication model introduced in Sect. 3 incorporates these relations. We proceed as follows: first, we will formalize properties of human visual object perception, to receive relevant mathematical relationships. Then we consider how these relations are represented in our model.

We focus on the 'atomic' perception, which involves the process of identifying a specific object within a specified period of time. It is important to note that the perception of objects in different times and spaces, i.e., object perception in a general sense, is beyond the scope of the current work.

Persons see and 'see' objects. In other words, they are doing two separate actions. First, they see, namely perceive objects using their designated devices – usually their eyes. Then, they become *aware* of that object. Further actions may be taken based on the perception to accomplish specific tasks. For example, imagine a situation in which a car is coming fast towards you. First, you see the car ('see'), then you identify the car approaching you ('aware'), and finally you step onto the sidewalk ('action'). Here we formalize the first two steps - 'see' and 'aware'.

The process of seeing the physical image x is complex and involves various stages of image processing, feature extraction, and visual perception mechanisms in the human visual system. It encompasses the physiological and cognitive processes through which the visual information from the image x is interpreted and translated into the perceived image $seen(x)$. This includes the extraction of relevant visual features, the integration of contextual information, and the interpretation of the visual scene based on the individual's cognitive processes and prior knowledge.

It's important to note that the process of seeing the image is subjective and may vary among individuals due to differences in their visual perception abilities, cognitive processes, and prior experiences. Factors such as lighting conditions, viewing distance, visual acuity, and cognitive biases can also influence the perceived image.

In our model, we conceptualize the process of 'seeing' the image as a series of successive image processing steps that generate a new image of similar modality. Note that in our considerations we assume that the internal perceived image is represented as mathematical object.²

Let x represent a specific image that is observed by a person. For example, x could be a digital image. The seeing process involves the conversion

²Thanks to Andres Luure for this remark.

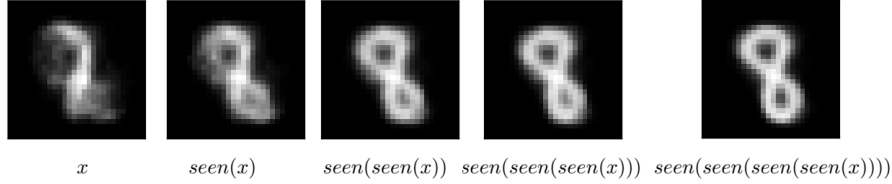


Figure 8: From left to right: the result of subsequent application of $seen$ operator observed in the experiments. Simulated is the visual perception of a person with the seen functionality biased to perception of even numbers.

of x into a perceived image denoted as $seen(x)$. We can treat $seen(x)$ as a new image, of similar modality, which represents the image that the person perceives. This conversion can be represented mathematically as:

$$x \rightarrow seen(x).$$

For example, x is a given image of a dog, and $seen(x)$ be an initial internal visual representation of the dog. Note that internal visual representation may differ from the initial one, but it is still an image.

The $seen$ function might be slightly distinct for different persons. For example, people may see dissimilar details in an observed image. Note that attention is only a part of the internal representation. This reflects the phenomena that people perceive objects differently.

Further, we formalize the process of seeing as sequential application of $seen$ function:

$$x \rightarrow seen(x) \rightarrow seen(seen(x)) \rightarrow \dots . \quad (28)$$

For example, during perception process of an image, its details may become clearer in a gradual fashion, this is illustrated at Fig. 8.

What are the equations that reflect the image perception awareness? Direct access to awarness metrics is hard (may involve operations procedures, or require dedicated equipment, that is expensive), therefore we use a mediated method of semantic analysis.

Consider the statement 'I see this image'. In this sentence, 'this image' has two meanings. First, it refers to the object itself (in the relevant modality). For example, an image of a dog. Second, it refers to an internal perceived image which is a translation of the original image. An inherent property of a consistent communication system is to make these two meanings close to each other, namely, to make \hat{x} equal to $seen(\hat{x})$:

$$seen(\hat{x}) = \hat{x} , \quad (29)$$

where \hat{x} is the final image representation referred as 'this image'. Detailed analysis of the meaning of the above sentence w.r.t. Eq. 29 is given in Appendix D.

Final representation of image perception is formalized as convergence

$$\lim_{n \rightarrow \infty} \text{seen}^{[n]}(x) = \hat{x} . \quad (30)$$

Summing up the above, seeing of visual objects may be formalized by:

- An operator $\text{seen}()$ acting in the image domain;
- Sequential application of $\text{seen}()$ to the initial image (Eq. 28).

In addition, awareness in perceiving of visual objects is formalized as:

- Convergence equation (Eq. 30);
- The fixed pointy property (Eq. 29).

How these properties are described by our model of Sect. 3? Equation 2 represents seen operator:

$$\text{obs} \rightarrow \text{seen} : \text{obs} \xrightarrow{\text{enc}} \text{enc}(\text{obs}) \xrightarrow{\text{dec}} \text{seen} = \text{dec}(\text{enc}(\text{obs})).$$

Step 3 of Algorithm 1 represents Eq. 28 at iter going to infinity. Equations 6 and 5 are related to convergence to attractors [28] and represent respectively Eqs. 29 and 30.

In such a way our model describes the following semiotic phenomena: the existence of the objects *seen* by a person, as well as the existence of objects the person *is aware of them* as such.

It is worth noting that although these aspects were not initially the primary focus of our attention, our model allows for the description of other semiotic aspects as well. We demonstrate this below

6.2 Person to person communication

In this section, we will explore how the semiotic properties of person-to-person communication are manifested in the communication model introduced in Sect. 3.

We analyze a sequence of 'transmitting' images that constitute the communication process and investigate how various semiotic properties are reflected in our model. In particular, we examine the sequence $U(Im)$ as

defined in Eq. 35, focusing on the properties of U that were discussed in Sect. 4.2.

Interpersonal dialogues can, after a certain point, become repetitive and circular. In our model, the process of interpersonal communication is always convergent, resulting in an orbit - a repetitive loop of images (Sect. 4.2.1). The phenomenon of converging dialogues to a cycle, starting at a certain point, is the first semiotic phenomenon of interpersonal communication modeled by our representation.

One of the semiotic properties of communication is that, during a dialogue, individuals perceive the objects of the interaction in a way that is unique to them, but this perception is also influenced by the other participant. In our model, this property is reflected in the structure of the personalized operators G_1 and G_2 of the seen in the dialog, defined as shown in Eqs. 10, 15:

$$G_1 = [F_1 \cdot F_2]^{K/2}, \quad G_2 = [F_2 \cdot F_1]^{K/2}, \\ \text{where } F_1 = [F_{P_1}]^{nsteps_1}, \quad F_2 = [F_{P_2}]^{nsteps_2}.$$

It should be noted that the values of F_{P_1} and $nsteps_1$ depend on person P_1 only but not on P_2 , and the same applies when swapping the indices 1 and 2. This highlights the uniqueness of each person in the dialog. However, the structure of the operators G_1 and G_2 also demonstrates that the way a person perceives the interaction is influenced by the other person, which reflects the aforementioned semiotic property. It is worth noting that our model reveals a non-obvious aspect of dialogues: not only does the content of a dialogue depend on the other participant ('what'), but also the way in which an individual perceives it can be influenced by the other participant ('how').

We may feel the entities of the dialog, yet they possess an elusive quality that may evade our conscious recognition. Similarly to person-object communication (Sect. 6.1), our awareness may be limited to the ultimate form of these entities. Let us show how this phenomenon is represented by our model.

The current discussion is focused on P_1 , but the same considerations are applicable to P_2 as well. Consider an inter-person communication dialog that begins with an image Im and a sequence $U(Im)$ of images transmitted during the dialog, as described in Eq. 35.

$$U(Im) = Im_1 \xrightarrow{[F_{P_1}]^{nsteps_1}} Im_2 \xrightarrow{[F_{P_2}]^{nsteps_2}} Im_3 \\ \xrightarrow{[F_{P_1}]^{nsteps_1}} Im_4 \xrightarrow{[F_{P_2}]^{nsteps_2}} Im_5 \xrightarrow{[F_{P_1}]^{nsteps_1}} \dots ,$$

Assuming that U is a bipartite convergent sequence of the first type (as defined in Definition 4.1), we consider an orbit of U as described in Statement 4.3. For every fixed point b_h in the orbit, where h is even, there exists a sub-sequence of U (as defined in to Eq. 11) that converges to b_h :

$$U_{b_h} = Im \xrightarrow{F_1} T_{1+0 \cdot K, P_1} \xrightarrow{F_2} \dots \xrightarrow{F_1} T_{1+0 \cdot K+h, P_1} \xrightarrow{G_1} \\ T_{1+1 \cdot K+h, P_1} \xrightarrow{G_1} \dots T_{1+2 \cdot K+h, P_1} \xrightarrow{G_1} \dots b_h$$

The outputs of operator G_1 in this sequence represent the entities that are *seen in the dialog* by person P_1 . This is analogous to the person-object communication discussed in Sect. 6.1. Specifically, the fixed point property of b_h expressed in Eq. 14:

$$G_1(b_h) = b_h$$

represents the person's awareness that the entity b_h is present in the dialogue.

The existence of both types of objects - those that are seen in the dialog and those that the person is aware of as the seen - represents the third semi-otic phenomenon of inter-person communication described by our model.

At times, the images that we see in the dialogue may be twofold. On one hand, we experience them as reflecting the view of the second person, as discussed earlier. In this sense, they are "imposed" on us. On the other hand, upon closer inspection, we may begin to feel that these images are actually our own, pre-existing before the start of the communication, with no connection to the other person. In this sense, our dialogue merely served as a pretext for their manifestation. Our model provides a representation of this phenomenon, shedding light on the complexities of inter-person communication, as supported by the following.

Consider what happens with the sequence $U(Im)$ when $nsteps_1$ and $nsteps_2$ increase. This may be seen as deeper processing by the individuals of the information received in interpersonal communication. As discussed in Sect. 4.2 (Statement 4.6), the orbits of the first type become closer to the second type. The former are comprised of the elements the person is aware of as seen in the dialog (as discussed above). The latter consist of attractors

b_h that satisfy Eq. 16:

$$\begin{aligned} F_{P_1}(b_h) &= b_h, \text{ for odd } h, \\ F_{P_2}(b_h) &= b_h, \text{ for even } h, \end{aligned}$$

where (Eq. 34):

$$F_{P_i} \text{ is composition } dec(enc) \text{ of } P_i, i = 1, 2.$$

As shown in Sect. 6.1 (Eq. 2), the attractors represent the objects that persons are aware of as seen. Attractors of a person do not depend on another person (in the autoencoder model, they depend on training data of the respective person) and do not depend on external input or other individuals. These attractors describe internal image representations that are inherently embedded within the person. However, the specific attractor to which the sequence converges depends on the input and the other person involved in the communication.

In such a way, our model represents the above phenomena: sometimes the communication dialogue serves just as a signal to 'wake up' one of the predefined internal representations. And this is the fourth phenomenon of inter-person communication described by our model.

7 Experimental Results

7.1 Implementation of Algorithm 1 for person-to-person communication

Our application implements Algorithm 1 for two-person communication. The autoencoders A_{P_1} and A_{P_2} were implemented following [5, 34], and trained at odd and even digits (30508 and 29492 images) from MNIST database [6] respectively. The autoencoders are Multi-Layer Perceptrons consisting of 6 hidden layers, with a depth of 512 units, and the latent space 2, trained at 20 epochs.

7.1.1 Attractors

In our experiments with attractors, we visualized the autoencoder latent space similarly to [5]: a rectangle covering the field of encoder values in the 2-dimensional latent space is partitioned by small squares. Each square is visualized by plotting the image obtained through the reconstruction decoder operation at the square's center.

To encounter the attractors, we randomly sampled 2000 points in the latent space of every autoencoder and iteratively applied the encoder-decoder iterations to each point until the consecutive vectors became sufficiently close. Each terminated vector was assigned to a predefined small bin in the latent space, where the bin corresponds to the location where the vector falls. The multiple elements falling into the same bin were considered as representing the same attractor. The number of counted elements in each bin indicates the cardinality of the respective attractor’s basin. The resulting distribution of counter values for the autoencoders is visualized in Fig. 9, where the bins are represented by circles with radii proportional to the bin counter.

For 247 samples, the sequences for autoencoder A_{P_1} did not converge to a fixed point. Instead, they exhibited convergence to a cyclic sequence. In Fig. 10, we visualize these cycles as follows: For every element in the cycle, we display its subsequent number within the cycle at the element’s location in the latent space.

These results demonstrate that memorization of training examples is not necessary for the convergence of encoding-decoding operations to attractors. Typically, the sequences started from random samples are converged to attractors, while in rare cases, they exhibit convergence to cycles.

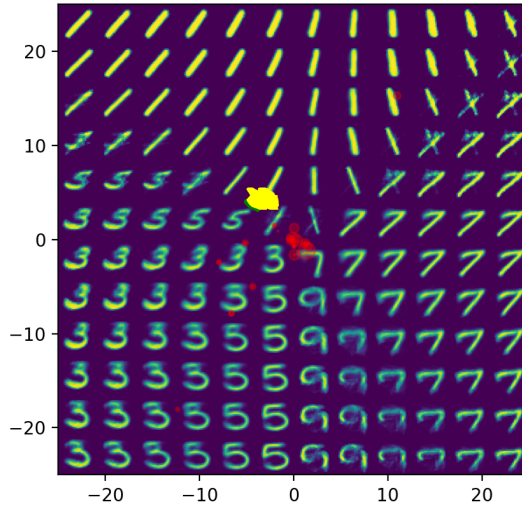
7.1.2 Bipartite Orbits

In our past experiments with the implementation of Algorithm 1, we varied the number of parameters $nsteps$ and initialization images. For each setting of $nsteps$, the observed orbits comprised a small set of orbits for a large set of initializations. The specific set of observed orbits depended on the starting image of the algorithm.

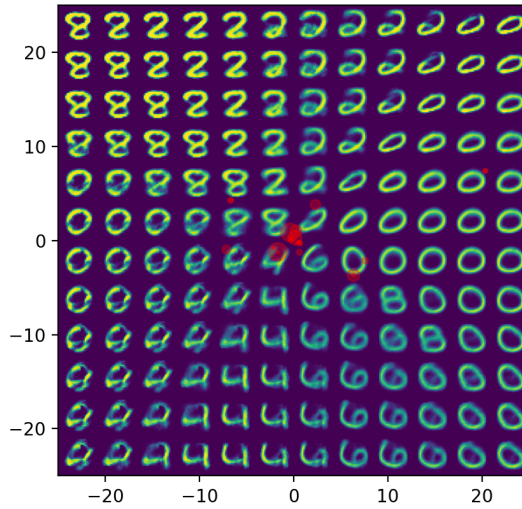
For example, Fig. 11 demonstrates a second type orbit of the person-to-person dialogue in Algorithm 1, implemented with autoencoders A_{P_1} and A_{P_2} . The values of $nsteps$ for P_1 and P_2 were set to 50. For such sufficiently large values, the final images of the sequence produced by the encoding/decoding operations in Step 3.2. of the algorithm became indistinguishable. The first type orbits become indistinguishable from the second type orbits.

7.2 Classifiers

We compared the performance of a standard MLP classifier M with our CONN vanilla and benchmark classifiers while training on datasets consist-



(A)



(B)

Figure (9): (Best viewed in color) Attractors yielded by autoencoders without memorization of the training examples. Red circles denote locations of the attractors, and the radii are proportional to the number of random samples falling into the attractor basins. (A) and (B): for autoencoders trained at odd and even RMNIST digits respectively. In (A), some samples result in sequences that converge to cycles, as shown in yellow. Refer to Fig. 10.

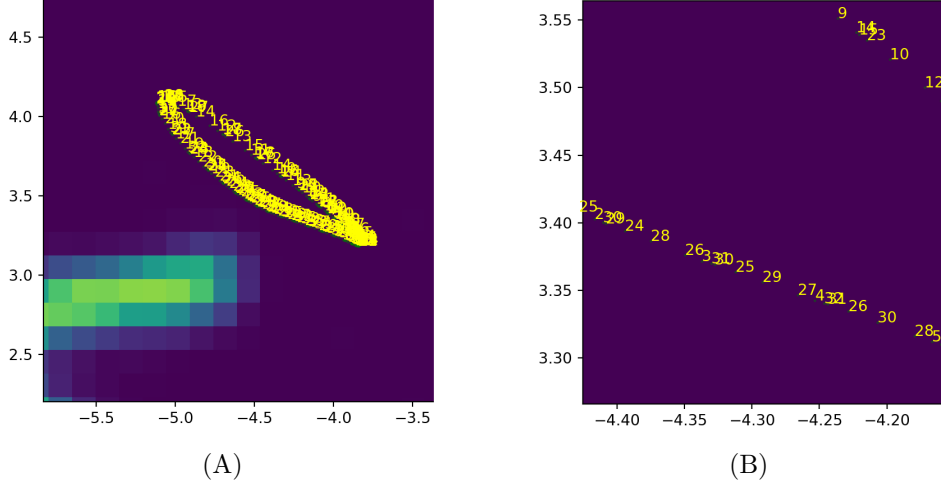


Figure 10: (Best viewed in color) The elements comprising the cycles of decoder/encoder operations for autoencoder A_{P_1} used in the experiments. (A) Yellow field ('ring') from Fig. 9,(A) in zoom. (B) A part of the 'ring' from (A) in zoom. See the text for further details.

ing of a small number of training examples.

The classifier M was trained at 40 training settings, produced by combinations of 10 training datasets and 4 numbers of training epochs. The training datasets TR were constructed by randomly selecting 5, 6, 7, 8, 9, 10, 20, 30, 40, and 50 examples for every digit from the MNIST training dataset, following [24, 25]. The number of training epochs was chosen as 25, 50, 100, and 200. The test set TE was constructed by randomly selecting 1000 examples from the MNIST test set.

For every training setting, we obtained the accuracies of M trained on the respective training set with the respective number of epochs, and tested it on the test set TE . See Fig. 6 (B).

Our vanilla and benchmark CONN classifiers incorporate fully convolutional autoencoders, similar to the autoencoder with the Cosid nonlinearity trained on MNIST images [29]. We trained the autoencoders with the same architecture on 10 training datasets TR , carefully tuning the hyperparameters to minimize the training error. For more detailed information, refer to Appendix G.

Furthermore, we mapped the training and test sets TR and TE to the training and test sets ATR and ATE 'seen' by the classifiers. See Fig. 6. The mapping was performed following Eqs. 26 and 27 for the vanilla and

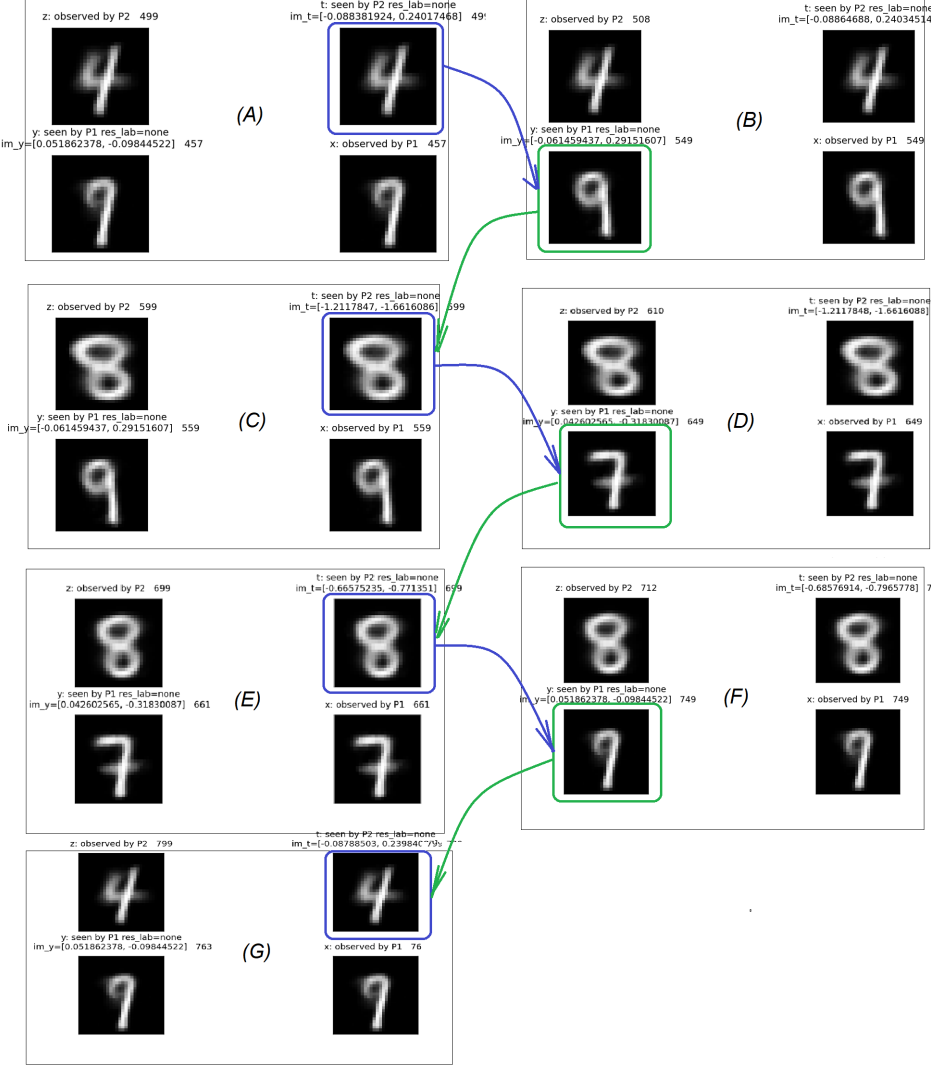


Figure 11: A bipartite orbit of the second type of the period length $K = 6$. (A)-(G): Subsequent temporal snapshots of the application implementing Algorithm 1. The arrows mark the Im_{iter} images transmitting between the persons (step 3.5. of the algorithm): blue and green arrows denote the images transferred from P_2 to P_1 and from P_1 to P_2 respectively. (A), (C), and (E): attractors for A_{P_2} forming the orbit. Note the difference between '8's depicted in (C) and (E). (B), (D), and (F): attractors for A_{P_1} forming the orbit.

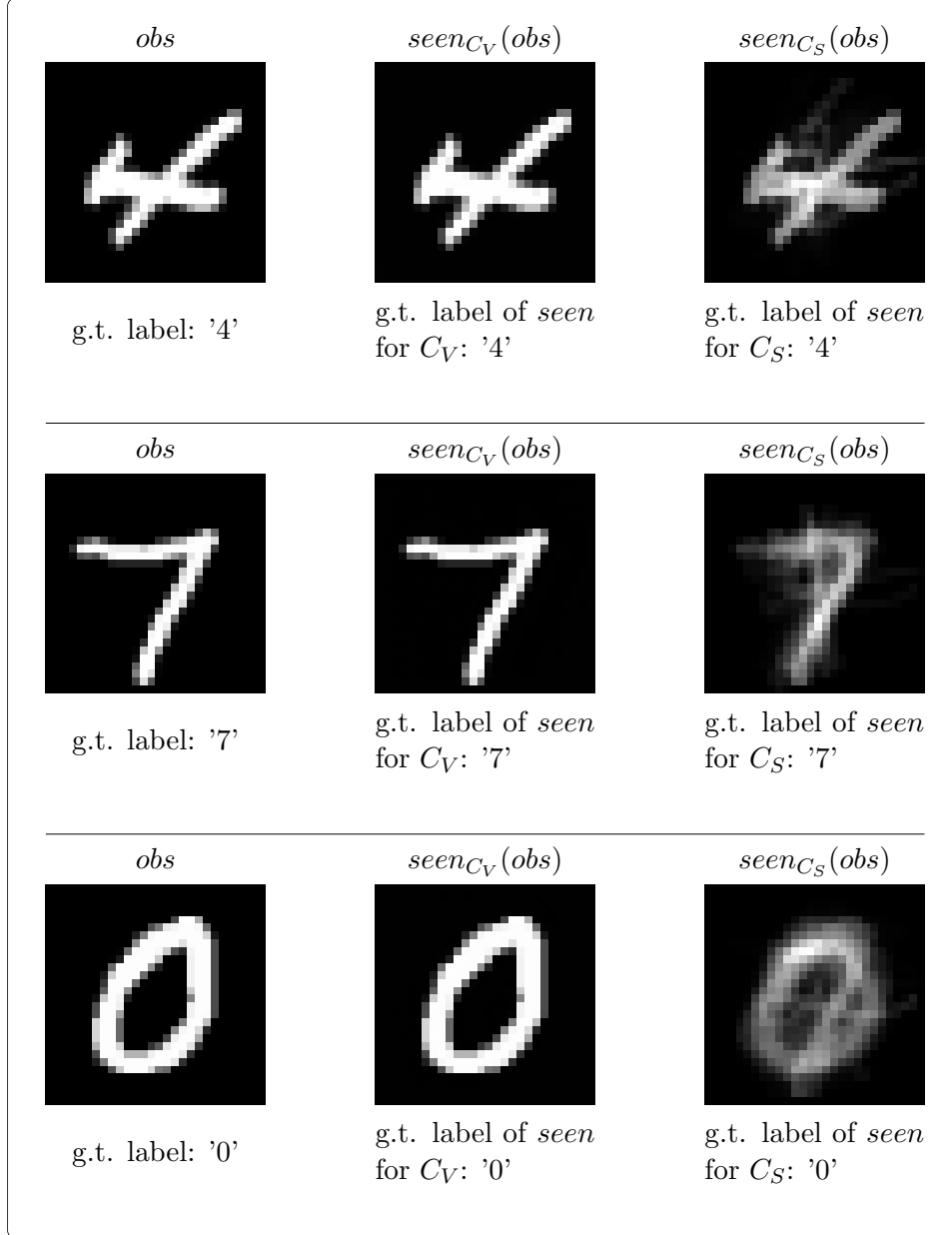


Figure 12: Examples of the images 'seen' by our vanilla classifier (second column) and stochastic classifier (third column) in our experiments for an 'observed' image from the train dataset (first column). The classifiers were trained for 200 epochs on the R8 restricted MNIST dataset [24, 25]. The $M(seen)$ denotes the label assigned by the benchmark classifier M to the 'seen' image, as shown at Fig. 6 (A)).

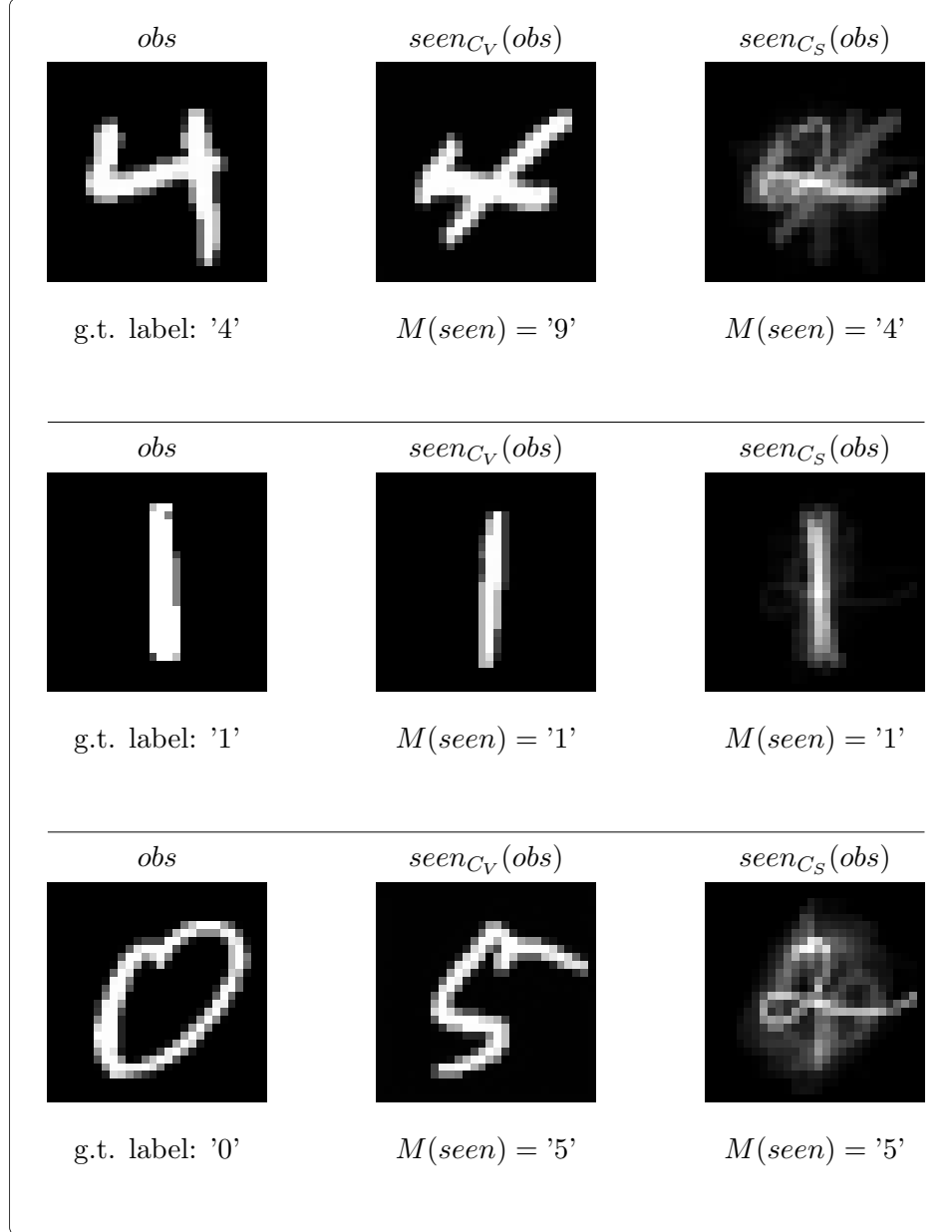
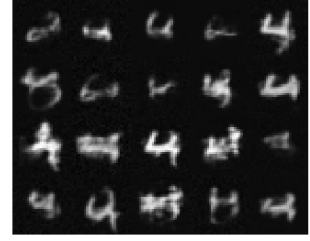


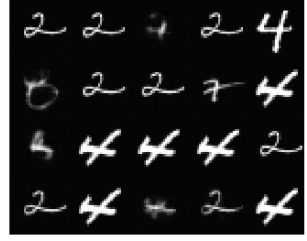
Figure 13: Examples of the images 'seen' by our vanilla classifier (second column) and stochastic classifier (third column) in our experiments for an observed image from the test dataset (first column). The vanilla classifier 'sees' in the observed image from the first row the memorized training example from the first row of Fig. 12. Construction of the seen images for the observed images from the first and second row is shown in Figs. 14 and 15 respectively. See capture of Fig. 12 for further details.



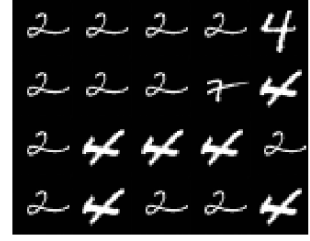
(A)



(B)

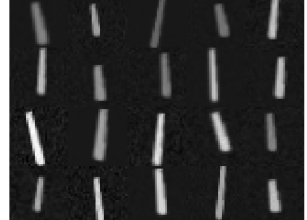


(C)

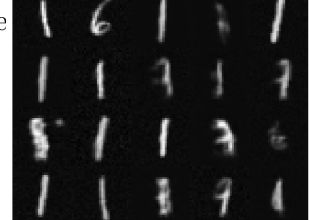


(D)

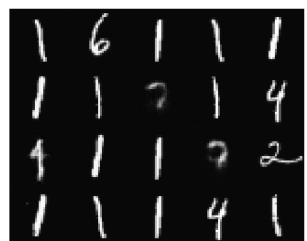
Figure (14): Construction of $seen_{CS}(obs)$ for the observed image by the stochastic classifier, shown in the upper row of Fig. 13. For each iteration, 20 images generated by Eq. 24 are displayed. (A) exhibits random augmentations of the input image before the $dec(enc())$ operation at the first iteration $i = 0$ of Eq. 24. Subsequently, (B), (C), and (D) depict the output at the 5th, and 14th iterations, re



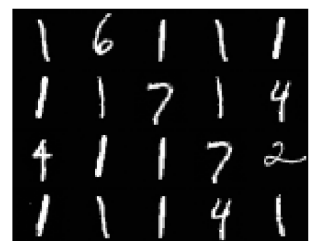
(A)



(B)



(C)



(D)

Figure (15): The same as Fig. 14, but for the 'observed' image by the stochastic classifier, shown in the middle row of Fig. 13.

stochastic classifiers, respectively. Examples of the images 'seen' by the CONN classifiers C are shown in Fig. 13.

Next, we obtained the performance results for both CONN classifiers by training M on sets ATR and testing it on ATE . The results are compared with the performance of M trained on datasets TR and tested on TE . The comparison demonstrates that the stochastic CONN classifier outperforms both the benchmark classifier and the vanilla CONN classifier. See Figs. 16 and 17.

Our benchmark classifier M , which is embedded in the vanilla and stochastic classifiers (Fig. 6), is a 3-layer MLP. It takes an input size of 28x28 pixels, has two hidden layers with widths of 500 and 100 neurons respectively, and has an output size of 10 classes.

The augmentations of the stochastic classifier (Eq. 24) were applied using [16]. The ensemble length J of Eq. 22 was set to 500, and the number of iterations (Eq. 23) to 30. The relaxator β of Eq. 25 was set to 2.6.

Furthermore, our experiments for stochastic classifiers were extended to reflect a certain dependence of the accuracies of the classifiers on the initialization of the networks. We performed 200 initializations for each considered training set TR , followed by testing on TE . We measured the mean and standard deviation of the respective accuracies of M (Fig. 6,(B)). Then we performed the same 200 initializations of M before training on ATR sets and measured the mean and standard deviation of the respective accuracies of M on the test set ATE .

The obtained results, shown in Figs. 16–19, confirm the outperformance of the stochastic classifier over the benchmark.

8 Discussion and Further Work

Our CONN model describes communication between individuals, where participants receive information in an external modality and convert it to an internal modality. Additionally, the participants are partially or fully conscious of the received information and exchange this perceived information with each other in the external modality. The model is structured as a sequence of observed and seen operations and employs subject-associated autoencoders for implementation. The input to the autoencoders consists of images in the external modality, while the latent space represents the internal modality.

Furthermore, the model also encompasses the perception of objects by individuals as a specific case.

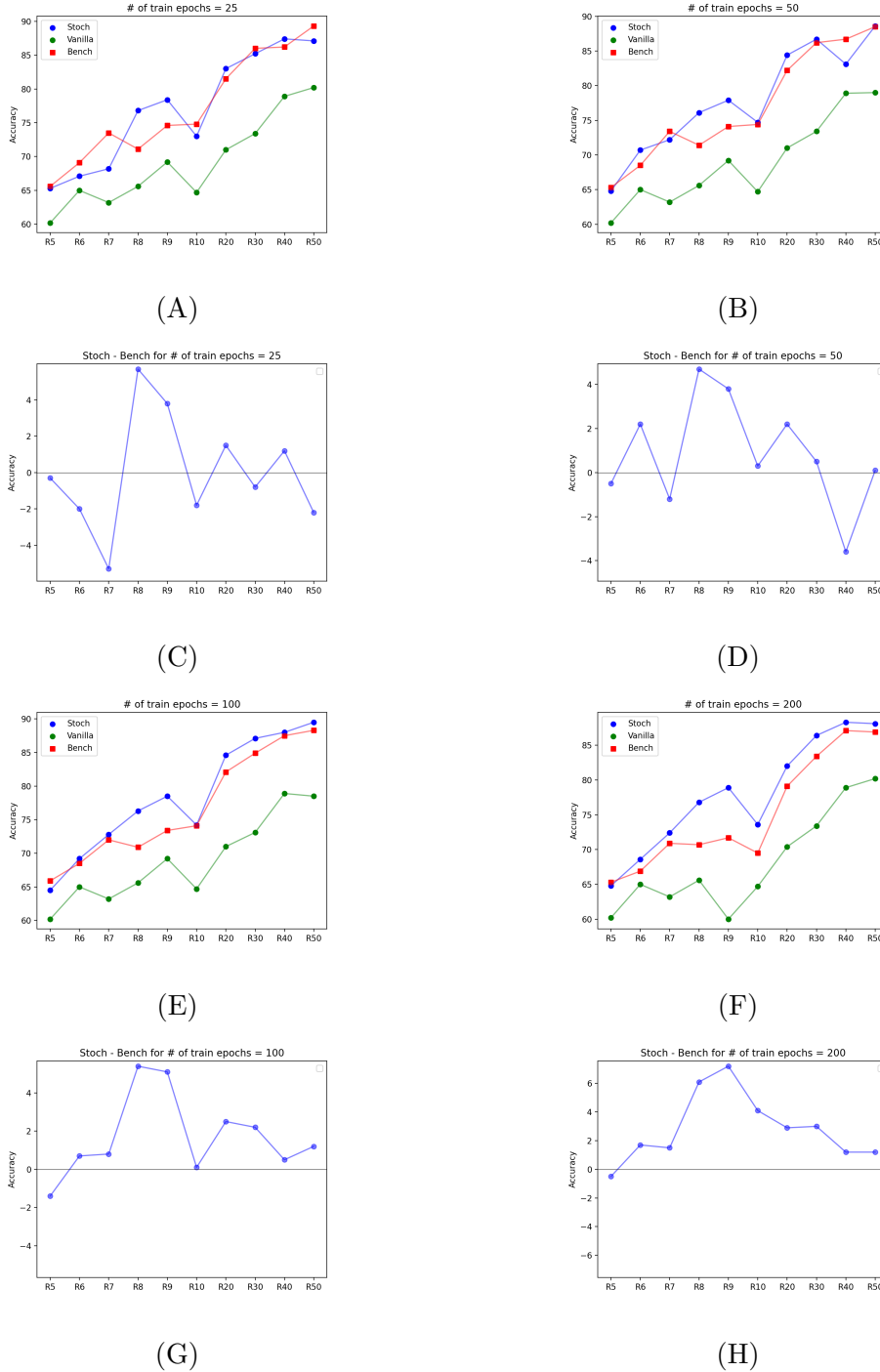
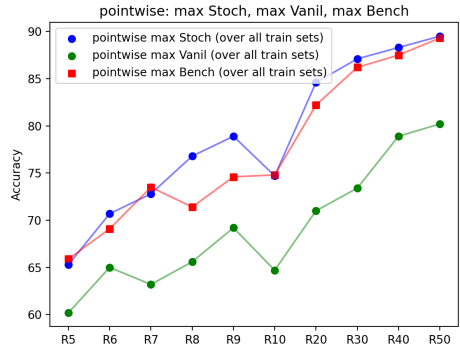
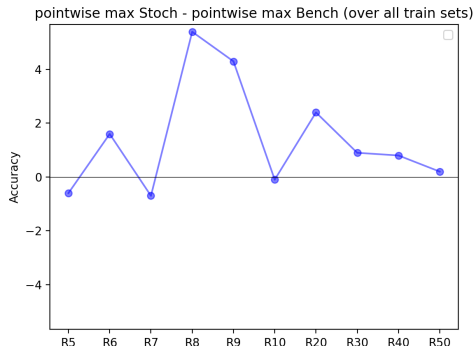


Figure (16): (Best viewed in color) (A), (B), (E), and (F): Comparison of accuracy between the stochastic CONN classifier (in blue), the vanilla CONN classifier (in green), and the benchmark classifier (in red) for different numbers of training epochs: 25, 50, 100, and 200, respectively. (C), (D), (G), and (H): Pointwise accuracy differences between the stochastic CONN classifier and the benchmark classifier for graphs (A), (B), (E), and (F), respectively. The x-axis tick values represent the size of the restricted MNIST training databases. For example, R10 corresponds to a training database comprising 10 examples per digit selected randomly from the training MNIST dataset [24, 25].



(A)



(B)

Figure (17): (Best viewed in color) Cumulative representation of the accuracy functions shown in Fig. 16. (A) Pointwise maxima of the accuracy functions for the stochastic CONN classifier (in blue), the vanilla CONN classifier (in green), and the benchmark classifier (in red) across the number of training epochs: 25, 50, 100, and 200. (B) Pointwise difference between the maximum functions of the stochastic CONN classifier and the benchmark classifier, as depicted in (A) for both classifiers. The x-axis tick values correspond to the size of the training databases, as in Fig. 16 .

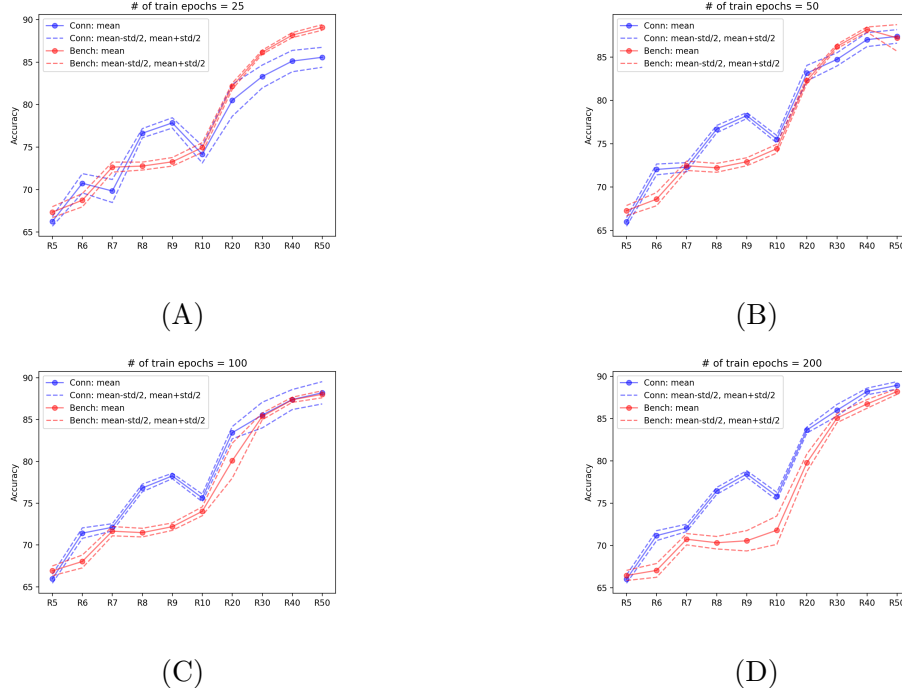


Figure (18): (Best viewed in color) (A), (B), (C), and (D): Average accuracy values for the stochastic CONN classifier (in blue), and the benchmark classifier (in red), over series of 200 random initializations before training, shown for different numbers of training epochs: 25, 50, 100, and 200, respectively. Dashed lines denote upper and lower bounds determined by half of the standard deviation. The x-axis tick values correspond to the size of the training databases, as in Fig. 16.

The CONNs simulate perceptual awareness in two aspects. Firstly, they model the observed/seen functionality of the visual perceptual awareness (Sect. 6.1). Additionally, they emulate the phenomenon of multistable human perception, which is elicited by ambiguous images such as the Rubin face-vase [39]. As discussed in Sect. 5.2, stochastic CONN classifier specifically emulates the properties of consistency and predefinency observed in human multistable perception. On the other hand, the importance of multistable perception for perceptual awareness has long been recognized [18, 21]. Recent neuroscience research establishes a connection between multistable phenomena and perceptual awareness, suggesting that multistability can play a crucial role in understanding the constructive process of perceptual inference [31]. Thus, CONN mimics multistable perception, which is recognized as essential for awareness. This represents the second aspect of CONN’s functionality in simulating awareness.

Under our model, the flow of information involved in perceiving an object by a person converges to a fixed point, which can be treated as a single-element cycle. This convergence characterizes the awareness of perceiving an object. Similarly, in the two-person communication model, we have experimentally observed and proven, under certain natural conditions, that the modeled flow of information between the participants exhibits the property of converging to a bipartite cycle (Statement [?]). In this sense, the bipartite orbits, when considered as a whole, can be seen as an ‘attractor of interpersonal communication’, representing what can be referred to as the collective consciousness?? within this communication.

We believe that our model can cope both full and partial awareness of perception. The model is mainly composed of two phases: internal phase and external one. The length of the internal phase directly affects awareness of the result it provided. We showed (Statement 4.6) that if $nsteps$ is large enough, convergence of the inter-person flow to bi-separation is guaranteed. Interestingly, even when $nsteps$ is as small as 1, where guarantees are not provided, bi-separations (Definitions 4.1) still occurs (see Sect. 4.2.1).

In a wide sense we may consider our model as decision-make. The model is composed of internal and external phases and can cope both short and long decision-making processes. The internal process is iterative and an inaccurate decision (but still valid) may result if the number of iterations is too small. Yet a valid decision can be returned at any time (iteration). This process can thus incorporate both fast and long decision-making procedures and can explain both reflexes and regular decisions, under the same procedure.

Our work explains that under certain conditions communication may not

Table 2: Types of CONN networks

Network Type	Definition and Properties	Models/Simulates	Performance of the CONN classifier at classification task with small training data w.r.t. a SOTA network: Sect.7
Vanilla	Person-Object: following [28]; Person-Person: Sects. 3 and 4.2	Modeling semiotic phenomena: Sect. 6	Underperforms
Stochastic	Person-Object: Sect. 5.2	Mimicking multistable perception: Sect. 5.2	Overperforms

be effective. Further research is required to explore which conditions need to be changed to better our communication channels. Furthermore, advertisers, sellers and any system that attempts to convince others to pursue any action, may use this work to design and test their messages. We offer a simulative test-ground and theoretical/experimental tool to study expected behaviors in communication situations.

Specifically, when designing a new item, such as furniture, clothing items, or a new car form, can we estimate how well its appearance will be received by the target audience? Ultimately, the acceptance of fashion-dependent objects relies on individuals' internal preferences, which are influenced by various factors and can change over time. It seems plausible to acquire knowledge about these preferences through observed/seen modeling. This can be achieved by training on streams of media data without processing input/output specifically associated with individual persons. Such an approach can be applied in the creation of fashion-dependent objects, including advertising imaging. Exploring this avenue is one of the directions of our research.

Our model may be applied to classical computer vision tasks, such as classification. Our CONN classifier, based on the one-person communication model, demonstrated superior performance compared to a SOTA neural

network classifier at classification tasks with small training data (Sect. 5).

For a given classifier M and training and test sets, our model offers an alternative approach to the conventional training and testing of the classifier. Instead, we convert the sets into their perceptual counterparts, which consist of images that the CONN network "perceives" in the original sets (as discussed in Sect. 5). Subsequently, classifier M is trained and evaluated on these transformed sets. The transformed sets can be considered as perceptual versions of the sets, framing the overall process as the "perceptualization of a classifier." Importantly, our experimental results demonstrate that this perceptualized version of the classifier consistently outperforms the original version across a range of small training datasets.

It may be noted that from an engineering perspective, the transition to the perceptual versions of the training and test sets can be interpreted as a preprocessing layer that precedes the input of data into the classifier.

The adaptability and flexibility of human perception in interpreting ambiguous visual stimuli considered above reflects the robustness and generalization abilities of the human visual system. Another manifestation of these abilities is resilience to adversarial attacks. It is widely acknowledged that human perception exhibits greater resilience against adversarial attacks compared to neural networks (see, for example, [26, 30]). Whether our classifier which mimics the properties of human perception is resilient to adversarial attacks?

A classical adversarial attack is one in which an input image with indistinguishable noise is given to a neural network and the network returns a wrong answer, while returning a correct answer to the original input image (without the additional noise). Humans are mostly immune to these kinds of attacks and therefore return the correct answer to both original and noised images. Many papers explored these [8–10, 22] attacks and attempted to offer a few approaches how to deal with them. Various approaches to achieving resilience in deep learning models have been proposed, including the use of autoencoders for denoising [2, 3] and ensembles [2, 19]. Another approach involves adding noise to the training examples [38], test examples [19], or both [33]. However, such approaches in general do not guarantee ideal defense, as demonstrated by the lack of a method demonstrating perfect resilience [37].

A classical adversarial attack occurs when a neural network receives an input image with indistinguishable noise and provides an incorrect answer, despite correctly classifying the original image without the additional noise. In contrast, humans are largely immune to these types of attacks and consistently provide correct answers for both the original and noised images.

Numerous papers have explored these attacks and have attempted to propose approaches to mitigate them (see [8–10, 22] for examples).

Various strategies have been proposed to enhance resilience in deep learning models. These include the use of autoencoders for denoising [2, 3], ensembles [2, 19], and the introduction of noise to training examples [38], test examples [19], or both [33]. However, it should be noted that these approaches do not guarantee ideal defense, as demonstrated by the absence of a method that provides perfect resilience [37].

In Section 2, it was noted that the primary difference between the vanilla CONN classifier and autoencoders [2, 3] is the iterative process of combining decoder and encoder operations (Eq. 2), leading to convergence towards attractors. This unique characteristic of the vanilla CONN classifier has the potential to hinder perturbation attacks on the classifier, as discussed in Sect. F.

The stochastic CONN classifier offer additional defensive measures. These mechanisms include employing ensemble methods and introducing noise during both the training and testing phases. Overall, we anticipate that designing a successful attack against stochastic CONNs would be exceedingly challenging due to the considered defense mechanisms.

Investigating and analyzing the resilience properties of our classifier in the face of various adversarial attacks forms another direction of our ongoing research.

Our work deals with one person perception (internal perception) and communication between two persons, but this model can be elaborated to more than two persons. In addition, it is not limited to persons and any system that has internal representation and a limited number of options (state machine) may use this work to further investigate its behavior. Note that the current system only supports the following conditions: 1) input and output modalities are the same, 2) it works in iterative (trainable) fashion. Under these conditions we show convergence of input to certain output (attractors, orbits). The further research is needed to relax these conditions.

Thanks to Prof. Andres Luure and Prof. Michael Bialy for their valuable contributions and insightful discussions. Special thanks to Nadav Kadvil for the fruitful discussions.

We acknowledge the use of Michael Nielsen’s GitHub repository [25] for the implementation of the restricted MNIST datasets in our work, and the Alexander Jung’s repository [16] used for image augmentations. We would like to acknowledge the following references for providing code examples that inspired and influenced the development of our CONN implementation:

[5, 7, 34]. Additionally, we would like to credit the Pixabay image collection [27] for providing the images used in this paper.

A Definition of the sequence U of the images transmuted between the persons in person-to-person CONN implemented using encoder/decoder operations

Human communication is simulating in our approach by transmitting images from one person to the other. The first step a person takes when receiving an image is transforming it to the latent space (Algorithm 1). Following the person yields the result of step 3.2.. Let $S_{iter, P_{i(iter)}}$ be the sequence of images generated in this operation (see Eq. 32), and W be all sequence of images (see Eq. 33), where $iter = 1, \dots, n_iters$ and

$$i(iter) = \begin{cases} 1, & \text{if } iter \text{ is odd} \\ 2, & \text{if } iter \text{ is even} \end{cases}. \quad (31)$$

The $iter$ refers to 'external' iteration and $i(iter)$ to the person's index. Let

$$\begin{aligned} S_{iter, P_{i(iter)}} &= Im_{iter}, [dec(enc)]^1(Im_{iter}), \dots, \\ Im_{iter+1} &= [dec(enc)]^{nsteps_{i(iter)}}(Im_{iter}), \end{aligned} \quad (32)$$

where dec and enc are encoding and decoding operations of $P_{i(iter)}$. Let

$$W(Im) = S_{1, P_1}, S_{2, P_2}, S_{3, P_1}, S_{4, P_2}, \dots, \quad (33)$$

where $Im = Im_1$. For example, S_{5, P_1} refers to the sequence of images in the fifth transaction of Person one.

Let

$$F_{P_i} \text{ be composition } dec(enc) \text{ of } P_i, i = 1, 2. \quad (34)$$

Consider the sequence of transmitting elements Im_{iter} in $W(Im)$:

$$\begin{aligned} U(Im) &= Im_1 \xrightarrow{[F_{P_1}]^{nsteps_1}} Im_2 \xrightarrow{[F_{P_2}]^{nsteps_2}} Im_3 \\ &\xrightarrow{[F_{P_1}]^{nsteps_1}} Im_4 \xrightarrow{[F_{P_2}]^{nsteps_2}} Im_5 \xrightarrow{[F_{P_1}]^{nsteps_1}} \dots, \end{aligned} \quad (35)$$

where $Im_1 = Im$.

B Partitioning a subsequence of U

We show below an example of partitioning the first $1 + (n + 1) * K$ members of sequence U (Eq. 11) by the first element of U (Im) following the matrix of $(n + 1)$ rows and K columns. For simplicity the arguments of U are not shown. The partitioning proceeds similarly to function *reshape* of Python. In our example $K = 2$ and $n = 2$. Using the Python notation for indexing of U :

$$\begin{aligned}
 U[0 : 1 + (n + 1) * K + 1] &= Im \xrightarrow{F_1} \\
 T_{1+0 \cdot K, P_1} \xrightarrow{F_2} T_{1+0 \cdot K+1, P_2} &\xrightarrow{F_1} \\
 T_{1+1 \cdot K, P_1} \xrightarrow{F_2} T_{1+1 \cdot K+1, P_2} &\xrightarrow{F_1} \\
 &\dots \\
 T_{1+n \cdot K, P_1} \xrightarrow{F_2} T_{1+n \cdot K+1, P_2} &.
 \end{aligned} \tag{36}$$

C Proof of Statement 4.3

If we denote

$$G_1 = [F_1 \cdot F_2]^{K/2}, G_2 = [F_2 \cdot F_1]^{K/2}.$$

(Eq. 15) then one may define the sequences L_n with G_1, G_2 acting on their elements as follows:

$$\begin{aligned}
 L_0 &= (T_{1+0 \cdot K, P_1} \xrightarrow{F_2} T_{1+0 \cdot K+1, P_2} \xrightarrow{F_1} \dots \xrightarrow{F_2} T_{1+0 \cdot K+K-1, P_2}) \\
 &\quad G_1 \downarrow \qquad \qquad \qquad G_2 \downarrow \qquad \qquad \qquad G_2 \downarrow \\
 L_1 &= (T_{1+1 \cdot K, P_1} \xrightarrow{F_2} T_{1+1 \cdot K+1, P_2} \xrightarrow{F_1} \dots \xrightarrow{F_2} T_{1+1 \cdot K+K-1, P_2}) \\
 &\quad G_1 \downarrow \qquad \qquad \qquad G_2 \downarrow \qquad \qquad \qquad G_2 \downarrow \\
 &\dots \\
 L_n &= (T_{1+n \cdot K, P_1} \xrightarrow{F_2} T_{1+n \cdot K+1, P_2} \xrightarrow{F_1} \dots \xrightarrow{F_2} T_{1+n \cdot K+K-1, P_2}) \\
 &\quad G_1 \downarrow \qquad \qquad \qquad G_2 \downarrow \qquad \qquad \qquad G_2 \downarrow \\
 &\dots \\
 b_0 &\qquad \qquad \qquad b_1 \qquad \qquad \qquad b_{K-1}
 \end{aligned} \tag{37}$$

Since G_1, G_2 are continuous, elements b_h are the fixed points [28] for G_1, G_2 , see Eq. 14. From the convergence of the columns of Eq. 37 to b_h and continuity of F_1, F_2 follows Eq. 13. This proves Statement 4.3.

D Derivation of Eq. 29 from analysis of the meanings a statement.

Consider the meanings of the statement 'I see this image'. One meaning is 'the result of my seeing is this image'. This implies equivalence between two images. The first one is what the person refers as 'I see'. This may be represented as the result of application of *seen* operator to some \hat{x} . The second image is 'this image'. In such a way the meaning may be expressed as

$$\text{seen}(\hat{x}) = \text{'this image'}$$

What is \hat{x} to whom the 'see' is applied? Note, that another meaning of 'I see this image' is 'see this image', i.e. 'see' is applied to 'this image'. This specifies \hat{x} :

$$\hat{x} \text{ is 'this image'}$$

In such a way there hold the fixed point property of Eq. 29:

$$\text{seen}(\hat{x}) = \hat{x} ,$$

E Proof of Statement 4.6 (See page 18.)

Statement E.1. *If the following assumptions hold:*

- (A1) both F_{P_1} , F_{P_2} determine finite numbers of attractors at X ;
- (A2) every attractor a of F_{P_1} (resp. F_{P_2}) with a certain vicinity $\delta(a)$ belongs to the basin of a certain attractor a' of F_{P_2} (resp. F_{P_1});
- (A3) X is limited set in a finite-dimensional normed space;
- (A4) convergence of F_{P_r} , $r \in \{1, 2\}$ to attractors is uniform: for any $\epsilon > 0$ there exist N such that for any $x \in X$ there hold

$$\text{dist}(F_{P_r}^{[n]}, \lim_{n \rightarrow \infty} F_{P_r}^{[n]}) < \epsilon$$

for any $n \geq N$,

then the sequence $U(\text{Im})$ (Eq. 35) is a sequence of the bipartite convergence of the second type, converging to a bipartite orbit consisting of attractors of F_{P_1} and F_{P_2} .

Proof. Clearly the set $X = \{Im\}$ of all images satisfies (A3).

- (B1) Take arbitrary $Im \in X$ and $\epsilon > 0$.
- (B2) If necessary, decrease ϵ to ensure that ϵ -balls around the F_{P_1} and F_{P_2} attractors do not intersect. We may do it by (A1).
- (B3) If necessary, decrease ϵ to ensure that for any attractor a of F_{P_r} ϵ -ball around a is a subset of the basin of a certain attractor of $F_{P_{\alpha(r)}}$, where

$$\alpha(r) = \begin{cases} 2, & \text{if } r = 1 \\ 1, & \text{if } r = 2 \end{cases}. \quad (38)$$

We may do it by (A2).

- (B4) Set $nsteps_{1,0}$ such that for any $nsteps_1 \geq nsteps_{1,0}$ hold

$$[F_{P_1}]^{nsteps_1}(Im) \in B_\epsilon(a_1) \quad (39)$$

- (B5) Set $nsteps_{1,1}, nsteps_{2,1}$ such that for any $nsteps_1 \geq nsteps_{1,1}, nsteps_2 \geq nsteps_{2,1}$, for any attractor a of F_{P_r} holds

$$F_{P_{\alpha(r)}}^{[nsteps_{\alpha(r)}]}(B_\epsilon(a)) \subseteq B_{\epsilon(a')}$$

where a' is a certain attractor of $F_{P_{\alpha(r)}}$. We may do it since, by (B2), $B_\epsilon(a)$ is included to a certain basin of $F_{P_{\alpha(r)}}$. We achieve inclusion to $B_{\epsilon(a')}$ by setting sufficiently large $nsteps_{1,1}, nsteps_{2,1}$ using uniform convergence to attractors (A4).

- (B6) Denote

$$F_1 = [F_{P_1}]^{nsteps_1}, F_2 = [F_{P_2}]^{nsteps_2}.$$

Also, for $x \in X, r = 1, 2$ denote attractor

$$A_r(x) = \lim_{n \rightarrow \infty} [F_{P_r}]^n(x),$$

- (B7) Consider sequence of attractors

$$a_1 = A_1(F_1(Im)), a_2 = A_2(F_2(a_1)), a_3 = A_1(F_1(a_2)), \dots \quad (40)$$

and ϵ -balls around them.

Since the ϵ -balls do not intersect (B2), by condition (A3), the number of different ϵ -balls in sequence $\{B_\epsilon(a_{niter})\}$ is finite. Thus, after a certain odd N , the sequence is repeated:

$$B_\epsilon(a_1), B_\epsilon(a_2), \dots, B_\epsilon(a_N), B_\epsilon(a_{N+1}), \dots, B_\epsilon(a_{N+K}) = B_\epsilon(a_N), \dots \quad (41)$$

Also, by (B5),

$$F_2(B_\epsilon(a_1) \subseteq B_\epsilon(a_2)), F_1(B_\epsilon(a_2) \subseteq B_\epsilon(a_3)), F_2(B_\epsilon(a_3) \subseteq B_\epsilon(a_3)), \dots \quad (42)$$

(B8) Consider sequence

$$U(Im) = Im \xrightarrow{F_1} T_{1,P_1} \xrightarrow{F_2} T_{2,P_2} \xrightarrow{F_1} T_{3,P_1} \xrightarrow{F_2} T_{4,P_2} \xrightarrow{F_1} \dots \quad (43)$$

(see Eq. 7).

Since $T_{1,P_1} = F_1(Im)$, by Eq. 39, $T_{1,P_1} \in B_\epsilon(a_1)$. Then, by Eq. 42, $T_{2,P_2} \in B_\epsilon(a_2)$, $T_{3,P_1} \in B_\epsilon(a_3)$, etc., i.e.

$$T_{niter,P_{i(niter)}} \in B_\epsilon(a_{niter}), \quad (44)$$

where $i(niter)$ is defined in Eq. 31. Then, by Eq. 41, for any $nsteps_1 >= nsteps_{1,1}, nsteps_2 >= nsteps_{2,1}$

$$\begin{aligned} T_{N,P_1} &\in B_\epsilon(a_N), & T_{N+1,P_2} &\in B_\epsilon(a_{N+1}), \dots, & T_{N+K-1,P_2} &\in B_\epsilon(a_{N+K-1}), \\ T_{N+K,P_1} &\in B_\epsilon(a_N), & T_{N+K+1,P_2} &\in B_\epsilon(a_{N+1}), \dots, & T_{N+2K-1,P_2} &\in B_\epsilon(a_{N+K-1}), \\ T_{N+2K,P_1} &\in B_\epsilon(a_N), & T_{N+2K+1,P_2} &\in B_\epsilon(a_{N+1}), \dots, & T_{N+3K-1,P_2} &\in B_\epsilon(a_{N+K-1}), \\ &\dots &&&& \end{aligned} \quad (45)$$

This proves bipartite convergence of the second type to a bipartite attractor. Since, by Eq. 41, the sequence $(a_N, a_{N+1}, \dots, a_{N+K-1})$ consists of the attractors of F_{P_1} and F_{P_2} , this proves the statement.

□

F Resilience to adversarial attacks of vanilla CONN classifier

Let Im , an input to the vanilla CONN classifier, be subjected to an adversarial attack. Our analysis is based on empirical evidence indicating

that overparameterized autoencoders typically map input examples to attractors [28] (see also Sect. 7). According to the classifier’s definition, the labeling assigned to Im by the CONN classifier is determined by the attractor $a = \hat{F}(Im)$ (see Sect. 5.1).

Let us consider a ball $B_{r_{\max}}(Im)$ with the maximum radius r , such that a ball $B_r(Im)$ centered at Im is completely contained within the basin [28] $BA(Im)$ of Im . It follows from the above that an attack leading to misclassification should replace Im with an image Im' located further from Im than $r_{\max}(Im)$. For sufficiently large values of r_{\max} , this ensures that Im' is distinguishable from Im , thereby preventing such attacks.

How large can be the values of $r_{\max}(Im)$? Experimental findings [28] demonstrate that the basins of an overparameterized autoencoder partition the image space with sharp/clearly delineated borders. The boundaries between the basins are well-defined and easily distinguishable, allowing for clear separation of the regions. This guarantees that many images Im are relatively distant from the borders of their basins, resulting in a relatively large value of $r_{\max}(Im)$. Consequently, it generally hampers perturbation attacks on the vanilla CONN classifier.

G Details of Training Overparameterized Autoencoders at Restricted RMNIST Datasets

The network consists of 14 layers with a depth of 256. During training, we used the Adam optimizer with a learning rate of 1e-5 and a seed of 3. The minibatch size was set to 4.

We trained the network on restricted MNIST datasets, as described in [24, 25], which are referred to in Table 3. For example, RMnist7 corresponds to a training database comprising 7 examples per digit selected randomly from the training MNIST dataset.

The training was done for 110,000 epochs, and the model that minimized the training error over the last 10,000 epochs was selected. The training error minimization approached the point of overfitting the training set. Due to resource limitations, we trained the autoencoders for a smaller number of epochs compared to [29]. As a result, our training errors are still higher than those reported there. Table 3 shows the minimal training errors attained for each restricted MNIST dataset.

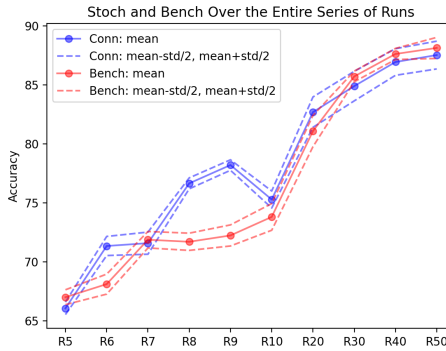


Figure (19): (Best viewed in color) Average accuracy values for the stochastic CONN classifier (in blue), and the benchmark classifier (in red), over series of 200 random initializations before training, and different numbers of training epochs: 25, 50, 100, and 200. Dashed lines denote upper and lower bounds determined by half of the standard deviation. The x-axis tick values correspond to the size of the training databases, as in Fig. 16.

Table 3: Training errors for the autoencoders trained at restricted MNIST datasets

RMnist5	RMnist6	RMnist7	RMnist8	RMnist9
0.03	0.04	0.04	0.04	0.04
RMnist10	RMnist20	RMnist30	RMnist40	RMnist50
0.04	0.04	0.04	0.03	0.04

References

- [1] Michael Biehl, Barbara Hammer, and Thomas Villmann. Prototype-based models in machine learning. *Wiley Interdisciplinary Reviews: Cognitive Science*, 7(2):92–111, January 2016.
- [2] Ka-Ho Chow, Wenqi Wei, Yanzhao Wu, and Ling Liu. Denoising and verification cross-layer ensemble against black-box adversarial attacks. In *2019 IEEE International Conference on Big Data (Big Data)*. IEEE, December 2019.
- [3] Antonia Creswell and Anil Anthony Bharath. Denoising adversarial autoencoders. *IEEE Transactions on Neural Networks and Learning Systems*, 30(4):968–984, April 2019.
- [4] Steve Dias Da Cruz, Bertram Taetz, Thomas Stifter, and Didier Stricker. Autoencoder attractors for uncertainty estimation. In *Proceedings of the IEEE International Conference on Pattern Recognition (ICPR)*, pages 2553–2560, 2022.
- [5] Alexander Van de Kleut. Variational autoencoders (vae) with pytorch. <https://avandekleut.github.io/vae/>, 2020.
- [6] Li Deng. The mnist database of handwritten digit images for machine learning research. *IEEE Signal Processing Magazine*, 29(6):141–142, 2012.
- [7] Shashank Dhar. A simple implementation of variational autoencoder algorithm (vae) using the mnist dataset. <https://github.com/shashankdhar/VAE-MNIST>, 2019.
- [8] El-Mahdi El-Mhamdi, Sadegh Farhadkhani, Rachid Guerraoui, Arsany Guirguis, Lê Nguyên Hoang, and Sébastien Rouault. Collaborative learning in the jungle (decentralized, byzantine, heterogeneous, asynchronous and nonconvex learning). In *Advances in Neural Information Processing Systems (NeurIPS)*, 2021.
- [9] Jonas Geiping, Liam Fowl, W. Ronny Huang, Wojciech Czaja, Gavin Taylor, Michael Moeller, and Tom Goldstein. Industrial scale data poisoning via gradient matching. In *International Conference on Learning Representations*, 2021.

- [10] Ian Goodfellow, Patrick McDaniel, and Nicolas Papernot. Making machine learning robust against adversarial inputs. *Communications of the ACM*, 61(7):56–66, 2018.
- [11] Amir Hossein Hadjahmadi and Mohammad Mehdi Homayounpour. Robust feature extraction and uncertainty estimation based on attractor dynamics in cyclic deep denoising autoencoders. *Neural Computing and Applications*, 31(11):7989–8002, July 2018.
- [12] Uri Hasson, Talma Hendler, Dafna Ben Bashat, and Rafael Malach. Vase or face? a neural correlate of shape-selective grouping processes in the human brain. *Journal of Cognitive Neuroscience*, 13(6):744–753, August 2001.
- [13] W. H. Ittelson. *Visual Space Perception*. Springer Publishing Company, 1969. LOCCCN 60-15818.
- [14] Klara Janglajew and Ewa Schmeidel. Periodicity of solutions of non-homogeneous linear difference equations. *Advances in Difference Equations*, 2012(1), November 2012.
- [15] Zee Julian. Osgood-schramm model of communication. In Editor Name, editor, *Key Concepts in Marketing*. SAGE Publications Ltd, 2009.
- [16] Alexander Jung. Image augmentation for machine learning experiments. <https://github.com/aleju/imgaug>, 2020.
- [17] David Kupeev. Alteregonets: a way to human augmentation, 2019.
- [18] David A. Leopold and Nikos K. Logothetis. Multistable phenomena: changing views in perception. *Trends in Cognitive Sciences*, 3(7):254–264, July 1999.
- [19] Jing Lin, Laurent L. Njilla, and Kaiqi Xiong. Secure machine learning against adversarial samples at test time. *EURASIP Journal on Information Security*, 2022(1), January 2022.
- [20] D.G. Lowe. Object recognition from local scale-invariant features. In *Proceedings of the Seventh IEEE International Conference on Computer Vision*. IEEE, 1999.
- [21] Erik D. Lumer, Karl J. Friston, and Geraint Rees. Neural correlates of perceptual rivalry in the human brain. *Science*, 280(5371):1930–1934, June 1998.

- [22] Aleksander Madry, Aleksandar Makelov, Ludwig Schmidt, Dimitris Tsipras, and Adrian Vladu. Towards deep learning models resistant to adversarial attacks, 2017.
- [23] Alexander Mordvintsev, Christopher Olah, and Mike Tyka. Inceptionism: Going deeper into neural networks, 2015.
- [24] Michael Nielsen. Reduced mnist: how well can machines learn from small data? <https://cognitivemedium.com/rmnist>, 2017.
- [25] Michael Nielsen. Rmnist repository. <https://github.com/mnielsen/rmnist>, 2017.
- [26] Nicolas Papernot, Patrick McDaniel, Somesh Jha, Matt Fredrikson, Z. Berkay Celik, and Ananthram Swami. The limitations of deep learning in adversarial settings. In *2016 IEEE European Symposium on Security and Privacy (EuroS & P)*. IEEE, March 2016.
- [27] Pixabay.com. Pixabay. <https://pixabay.com/>, 2023.
- [28] Adityanarayanan Radhakrishnan, Mikhail Belkin, and Caroline Uhler. Overparameterized neural networks implement associative memory. *Proceedings of the National Academy of Sciences*, 117(44):27162–27170, 2020.
- [29] Adityanarayanan Radhakrishnan, Mikhail Belkin, and Caroline Uhler. Supplementary information for overparameterized neural networks implement associative memory. www.pnas.org, 2023.
- [30] Huali Ren and Teng Huang. Adversarial example attacks in the physical world. In *Machine Learning for Cyber Security*, pages 572–582. Springer International Publishing, 2020.
- [31] Chiara Saracini. Perceptual awareness and its relationship with consciousness: Hints from perceptual multistability. *NeuroSci*, 3(4):546–557, October 2022.
- [32] Yantao Shen, Hongsheng Li, Tong Xiao, Shuai Yi, Dapeng Chen, and Xiaogang Wang. Deep group-shuffling random walk for person re-identification, 2018.
- [33] Lin Shi, Teyi Liao, and Jianfeng He. Defending adversarial attacks against DNN image classification models by a noise-fusion method. *Electronics*, 11(12):1814, June 2022.

- [34] Aaron Stone, Richard Kalehoff, Jacob Walker, Islam Al-Afifi, and Patrick Donovan. Pytorchcrashcourse. <https://github.com/udacity/pytorchcrashcourse>, 2022.
- [35] University of Minnesota Libraries Publishing Edition. Communication in the real world: An introduction to communication studies. <https://open.umn.edu/opentextbooks/textbooks/274>, 2016.
- [36] Ruben S. van Bergen and Janneke F.M. Jehee. Probabilistic representation in human visual cortex reflects uncertainty in serial decisions. *Journal of Neuroscience*, 39(41):8164–8176, October 2019.
- [37] Yulong Wang, Tong Sun, Shenghong Li, Xin Yuan, Wei Ni, Ekram Hossain, and H. Vincent Poor. Adversarial attacks and defenses in machine learning-powered networks: A contemporary survey, 2023.
- [38] Zhonghui You, Jinmian Ye, Kunming Li, Zenglin Xu, and Ping Wang. Adversarial noise layer: Regularize neural network by adding noise. In *2019 IEEE International Conference on Image Processing (ICIP)*. IEEE, September 2019.
- [39] Michael Zhu, Richard Hardstone, and Biyu J. He. Neural oscillations promoting perceptual stability and perceptual memory during bistable perception. *Scientific Reports*, 12(1), February 2022.

Supplementary Information for

Interpretable Semiotics Networks Representing Awareness

David Kupeev^{*1} and Eyal Nitcany²

¹Independent Researcher, Israel: kupeev@gmail.com

²Independent Researcher, Israel: eyalni@gmail.com

A Remarks on Bipartite Orbits

For a bipartite sequence $U(Im, nsteps_1, nsteps_2)$ alternation of $nsteps$ parameters typically leads to alternation of the period K . This is illustrated at Fig. 2 where elements of U visually undistinguishable from the bipartite orbit (see Fig. 1) of period $K = 4$ are shown. The orbit can not be the orbit for a larger value of $nsteps_{P_1}$ mapping T_{N+2, P_1} , located in the left basin of P_2 , to the right.

B Simple Modeling the Sequence of Interperson-Transmitted Images

Below, we describe a simple algorithm that constructs a sequence which, in some aspects, is similar to the sequence U described in Eq. ??). In this model, convergence to the 'attractors' (which are the numbers in R^2) is represented as a simple operation in a 2D linear space, without the usage of an autoencoder. Let N_1 and N_2 be predefined numbers of attractors for P_1 and P_2 , respectively. We consider a rectangle $R = [0; 1] \times [0; 1]$ and define the basins of attractors for P_1 by randomly partitioning R into N_1 rectangles stacked vertically. Similarly, we define the basins for attractors of P_2 by randomly partitioning R into N_2 rectangles stacked horizontally. This partitioning is illustrated in SI Supplementary Text B. Next, we randomly select one point in each basin to represent the attractor. Additionally, we choose a positive value k that is less than 1. Our modeling of the attractor related properties is described in Algorithm 1. One may see that

^{*}Corresponding Author

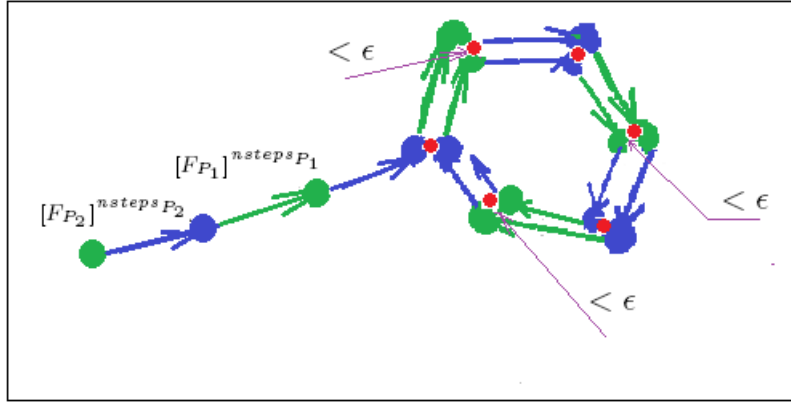


Figure 1: Illustration of bipartite orbit for (A) The bipartite orbit of the first type, for n_{iter} tending to infinity, (B) The bipartite orbit of the second type, for n_{iter} , n_{steps_1} , and n_{steps_2} tending to infinity. Elements of the bipartite orbit are shown in red. .

the transformation $Im_{iter} \rightarrow Im_{iter+1}$ in of the algorithm is described by a function $f_1(I)$ for odd values of $iter$ and by a function $f_2(I)$ for even values of $iter$. It worth to note that in difference to autoencoder functions, f_1 and f_2 are not continuous. Our simple modeling may be easily extended to continuous functions. One can observe that the transformation $Im_{iter} \rightarrow Im_{iter+1}$ in Equation 3.1. of the algorithm is described by the function $f_1(I)$ for odd values of $iter$ and by the function $f_2(I)$ for even values of $iter$. It is worth noting that unlike autoencoder functions, f_1 and f_2 are not continuous. However, our simple modeling approach can be easily extended to the iterations $Im_{iter} \rightarrow Im_{iter+1}$ described by continuous transformations f_1 and f_2 . In our experiments with the model, we consistently observed convergence to cycles of even length for every initial point I and value of k .

C Multiperson Attractor Algebra

First, we introduce the algebra for the first type orbits and then for the second.

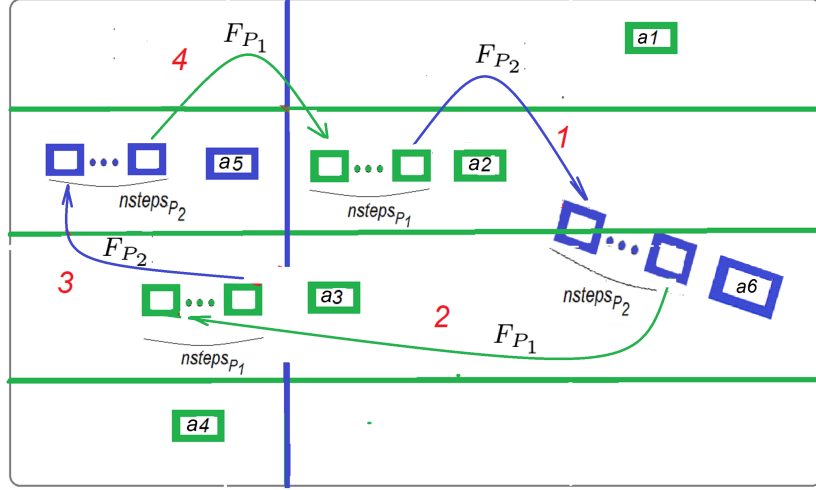


Figure 2: The image space is partitioned by four attractors basins of P_1 shown in green. The same image space is partitioned by two attractors basins of P_2 shown in blue. A Bipartite orbit of the first type of degree of 4: The red numbers denote transitions as follows: $T_{N,P_1} \xrightarrow{1} T_{N+1,P_2} \xrightarrow{2} T_{N+2,P_1} \xrightarrow{3} T_{N+3,P_2} \xrightarrow{4} T_{N+4,P_1}$ (Subsequences S_{N,P_1} and S_{N+4,P_1} are indistinguishable in the figure.) A bipartite orbit of the second type of degree 2: $a_5 \xrightarrow{1} a_2 \xrightarrow{2} a_6 \xrightarrow{3} a_3 \xrightarrow{4} a_6$.

Algorithm 1 Simple modeling of the attractor related properties of the sequence of interperson-transmitted images.

Input: a point $I \in R = [0; 1] \times [0; 1]$ which is related to person P_1

Output: A sequence of transaction points $I_1, I_2, \dots, I_k, \dots$

1. Set $iter = 1$;
2. Set $person_id = 1$;
3. While $iter <= n_iters$ do:
 - 3.1. Use $person_id$ parameters ($nsteps_{person_id}$);
 - 3.2. construct Im_{iter+1} such that $\overrightarrow{(Im_{iter}, Im_{iter+1})} = k \cdot \overrightarrow{(Im_{iter}, Att_{person_id}(Im_{iter}))}$
 - 3.3. Increase $iter$ by 1 and change $person_id$ to other $person_id$
 - 3.4. Send Im_{iter} to the updated person and return to step ??

C.1 The second type orbit algebra

Consider the 'limit case' of

$$U(Im) = Im_1 \xrightarrow{[F_{P_1}]^{nsteps_1}} Im_2 \xrightarrow{[F_{P_2}]^{nsteps_2}} Im_3 \xrightarrow{[F_{P_1}]^{nsteps_1}} \dots, \quad (1)$$

$$\xrightarrow{[F_{P_1}]^{nsteps_1}} Im_4 \xrightarrow{[F_{P_2}]^{nsteps_2}} Im_5 \xrightarrow{[F_{P_1}]^{nsteps_1}} \dots,$$

where $Im_1 = Im$ at $nsteps_1, nsteps_2$ tending to infinity.

Consider sequence:

$$\widehat{U}(Im) = Im \xrightarrow{\widehat{F}_1} a_{1,1} \xrightarrow{\widehat{F}_2} a_{2,2} \xrightarrow{\widehat{F}_1} a_{3,1} \xrightarrow{\widehat{F}_2} a_{4,2} \xrightarrow{\widehat{F}_1} \dots, \quad (2)$$

where $\widehat{F}_i(Im)$ are defined in

$$\widehat{F}_i(Im) = \lim_{n \rightarrow \infty} [F_{P_i}]^n(Im); \quad (3)$$

and F_{P_i} in

$$F_{P_i} \text{ be composition } dec(enc) \text{ of } P_i, i = 1, 2. \quad (4)$$

This sequence represents the sequence of Eq. 1 at $nsteps_1, nsteps_2 \rightarrow \infty$.

Here

$$a_{j,i(j)} \in A_{i(j)}, j = 1, 2, \dots. \quad (5)$$

Let

$$A = A_1 \cup A_2$$

and

For $a \in A$, define a monounary operation

$$\widehat{FM}(a) = \begin{cases} \widehat{F}_2(a), & \text{if } a \in A_1 \setminus A_2 \\ \widehat{F}_1(a), & \text{if } a \in A_2 \setminus A_1 \\ a, & \text{if } a \in A_2 \cap A_1 \end{cases} \quad (6)$$

This defines monounary algebra

$$\mathcal{A} = (A, \{\widehat{FM}\}).$$

We call this the multiperson attractor algebra (MAA).

It may be seen that $\widehat{U}(Im)$ may be represented as

$$\widehat{U}(Im) = Im \xrightarrow{\widehat{F}_1} a_{1,1} \xrightarrow{\widehat{FM}} a_{2,2} \xrightarrow{\widehat{FM}} a_{3,1} \xrightarrow{\widehat{FM}} a_{4,2} \xrightarrow{\widehat{FM}} \dots. \quad (7)$$

For $x, y \in A$ define a binary relation

$$x \sim y : \text{if exist } n_x, n_y \text{ such that } [\widehat{FM}]_x^n(x) = [\widehat{FM}]_y^n(y).$$

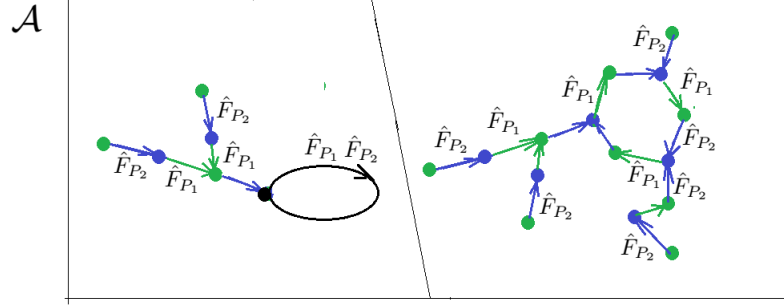


Figure 3: An example of the attractor algebra, denoted by \mathcal{A} , partitioned into two themes.

It may be easily shown that \sim is an equivalence relation on \mathcal{A} .¹ We call every equivalence class of \sim -relation the *theme* on \mathcal{A} , and for every $a \in \mathcal{A}$ the theme of \mathcal{A} containing a the *theme of a* .

The following statements are obvious.

Statement C.1. *For any $a \in \mathcal{A}$, the sequence*

$$a \xrightarrow{\widehat{FM}} a_1 \xrightarrow{\widehat{FM}} a_2 \xrightarrow{\widehat{FM}} \dots . \quad (8)$$

is a subset of the theme of a . \square

Statement C.2. *For $a \in \mathcal{A}$, $\widehat{FM}(a) = a$ if and only if $a \in A_1 \cap A_2$.* \square

Statement C.3. *If \mathcal{A} is finite, every theme \mathcal{T} of \mathcal{A} is connected digraph relatively \widehat{FM} operation, terminated by a loop L . The L is the unique loop in \mathcal{T} . The length $\text{len}(L)$ is even or is equal to 1. If $\text{len}(L)$ is even, L is comprised of alternating elements of A_1 and A_2 .* \square

An example of MAA comprised of two themes is shown at Fig. 3.

Statement C.4. *A theme \mathcal{T} on \mathcal{A} is a sub-algebra of \mathcal{A}* \square

This explains the term *theme*. The 'dialog' operations \widehat{F}_1 , \widehat{F}_1 partition the set of attractors of \mathcal{A} by the 'themes' \mathcal{T} , application of these operations to elements of every \mathcal{T} does not take us outside the theme, and lead to the circle of the theme.

¹The \sim is a congruence relation on \mathcal{A} : $\sim = (\widehat{F}_1 \vee \widehat{F}_2)$. For any $x \in \mathcal{A}/\sim$ there hold $\widehat{FM}(x) = x$.

C.2 The first type orbit algebra

Statement C.5. *Operation F_2 transfers a fixed point of G_1 to a fixed point of G_2 , operation F_1 transfers a fixed point of G_2 to a fixed point of G_1 , where*

$$F_1 = [F_{P_1}]^{nsteps_1}, F_2 = [F_{P_2}]^{nsteps_2}, \quad (9)$$

$$\begin{aligned} G_1 &= [F_1 \cdot F_2]^{K/2}, \\ G_2 &= [F_2 \cdot F_1]^{K/2}. \end{aligned} \quad (10)$$

Proof. For a a fixed point g_1 of G_1

$$(F_1 F_2 \dots F_1 F_2)(g_1) = g_1$$

thus

$$F_2(F_1 F_2 \dots F_1 F_2)(g_1) = F_2(g_1)$$

thus $F_2(g_1)$ is a fixed point of $G_2 = F_2(F_1 F_2 \dots F_1)$. \square

This allows to define, similarly to C, the algebra of fixed points of G_1, G_2 .
Let

$$E = E_1 \cup E_2$$

where E_1, E_2 are the fixed pints of G_1, G_2 respectively. For $e \in E$, define a monounary operation

$$FM(a) = \begin{cases} F_2(e), & \text{if } e \in E_1 \setminus E_2 \\ F_1(e), & \text{if } e \in E_2 \setminus E_1 \\ e, & \text{if } e \in E_2 \cap E_1 \end{cases} \quad (11)$$

By the above statement this defines a monounary algebra

$$\mathcal{E} = (E, \{FM\}).$$

We call this the multiperson algebra of fixed points.

Similarly to C, it is easily shown that

Statement C.6. *The sequence*

$$b_0, \dots, b_{K-1}$$

of Eq. 10 forms a loop in a theme of an monounary algebra of fixed points of G_1, G_2 . \square

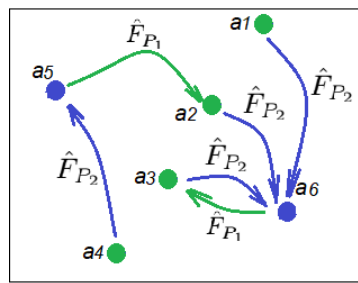


Figure 4: Multiperson Attractor Algebra for the attractors shown at Fig. 2.
Attractors A_1, A_2, A_3 and A_4